Probing Charge Transport in Molecular Junctions

by

Aaron Christopher Tan

A dissertation submitted in partial fulfillment
of the requirements for the degree of
Doctor of Philosophy
(Materials Science and Engineering)
in the University of Michigan
2012

Doctoral Committee:

Professor Peter F. Green, Co-Chair
Assistant Professor Pramod Sangi Reddy, Co-Chair
Assistant Professor Vikram Gavini
Assistant Professor Anton Van der Ven

Table of Contents

List of Figures

.

List of Appendices

Abstract

We present experimental work with a new atomic force microscope-based technique that attempts to elucidate the electronic structure of aromatic metal-molecule-metal junctions. In addition, we have also used this technique to perform preliminary studies on the relationship between the thermoelectric properties of molecular junctions and their molecular structure, the coupling strength of molecules to the electrodes, and the end groups of the molecule. The low-bias electrical conductance of junctions was found to be exponentially dependent on length and strongly affected by the coupling strength of the molecules to the electrodes. The low-bias electrical conductance of junctions was found to be exponentially dependent on length and strongly affected by the coupling strength of the molecules to the electrodes. The current-voltage characteristics of junctions of various molecular lengths were also analyzed using transition voltage spectroscopy. The transition voltage was found to decrease with increasing molecular length, indicating that the energetic separation between the chemical potential and the closest molecular orbital decreases with increasing length. Secondly, based on an analysis of our thermopower measurements using the Landauer model, electronic transport through aromatic thiols of various chain lengths was deduced to be HOMO dominated. The Seebeck coefficients for a series of dithiol molecules were also measured and were almost identical to corresponding values of the monothiol series. This suggests that coupling strength does

not play a role in the magnitude of a junction's thermopower, or equivalently, that the relative electronic alignment of molecular orbitals with respect to the Fermi level of the electrodes is unchanged by coupling strength. However, contact chemistry can play a significant role in molecular level alignment, as evidenced by the change in sign of the thermopower of a junction formed from an isocyanide-terminated monolayer. This sign change suggests a shift from HOMO- to LUMO-mediated transport in isocyanide molecules.

Chapter 1

Introduction

The benefits of organic electronics have already been utilized by many present-day technologies[1]. Devices such as organic light-emitting diodes[2,3], transistors [4,5], and solar cells[6-8] have appeared on the market as lightweight, low-cost, and flexible alternatives to traditional semiconductor based devices.

A promising next step in downsizing organic electronic systems is to reduce the size of the system from the bulk or thin film level to the scale of one or a small number of molecules. The use of molecules as electronic devices was first suggested by Mark Ratner and Avi Aviram in 1974[9], when they suggested that a molecular structure that could act as a diode and further described the theory that supported the plausibility of this proposal. Development in this field was rather slow, with very little experimental work done until the early 1990's.

As the size of electronic devices continues to decrease, quantum effects at the molecular level must be taken into consideration. In particular, understanding the energetic structure of organic molecules is important in designing novel materials for electronic applications in the future. This question has been an important focus of the field of molecular electronics for close to half a century.

The purpose of this investigation was to experimentally probe the electronic structure of prototypical organic metal-molecule-metal junctions (MMMJs). A new experimental atomic force microscope-based method was developed that allows for straightforward thermoelectric measurements of a small number of molecules assembled into a monolayer on a conductive surface. Information about the electronic structure of these MMMJs will be extracted from measurements of the current-voltage characteristics as well as the thermoelectric properties of these materials. We will also study the effects of the chemical structure on the thermoelectric properties of these junctions by systematically modifying the length and terminating groups of the molecules used.

In this introductory chapter, we will describe first the history of how organic molecules came to be thought of as potential media for transporting charge and energy. We will conclude this chronological description with a detailed overview of the present-day understanding of molecular conduction utilizing the Landauer model of transport. After this, a brief introduction to thermoelectricity will be given, as one of the critical measurements of this current work is measuring thermopower (Seebeck coefficient) at the molecular level. We will derive an expression for the Seebeck coefficient of a molecular junction within the Landauer model. Also, we describe an analysis technique for electron transport properties called transition voltage spectroscopy (TVS) that can help us understand the electronic structure of metal-molecule-metal junctions.

HISTORY

Although many reviews begin with Aviram and Ratner's work suggesting the possibility of using organic molecules as electronic components, it is noteworthy that the electrical properties of organic systems were already being considered in the first half of the 20th

century[10]. Mulliken was the first to propose the idea that organic molecules could serve as media for charge transport in 1939[11]. A spectroscopist, he investigated the electromagnetic emissions of small organic molecules that resulted from the molecule releasing energy as its electrons transfer from being in a high-energy molecular orbital (a term and concept that he had developed only six years earlier to describe a particular quantum probability distribution of electronic charge in a molecule) to a more stable, lower-energy orbital. Using a semi-classical description, this can correspond to the exchange or transfer of an electron between or amongst different atoms in a molecule. Charge transport through small molecules was studied over the next few decades, and resulted in the 1973 synthesis of the first highly conductive (metallic) organic crystal[12]. Comprised of an electron donor (tetrathiofulvalene, TTF) and acceptor (tetracyano-*p*-quinodimethane, TCNQ), the conductivity of the crystal came close to that of copper.

At the same time as charger transfer through organic and biological molecules was being studied, the importance of coupling to electron transfer was being considered. Henry Taube first published a paper on the effect of bridge type on electron transfer rate[13]. Before, the coupling in donor-acceptor complexes was considered to be rigid. Now, the model included a bridge (e.g. a molecule) that was connected between the donor and acceptor.

The idea of using organic molecules as electrical components was first proposed by Aviram and Ratner in 1974[9]. They proposed that organic compounds could be designed to perform many of the same basic operations that inorganic systems achieve in modern-day computers. The theoretical single-molecule rectifier structure was composed of a

TTF donor and TCNQ acceptor weakly linked by a carbon bridge. This molecule was experimentally verified to exhibit diode-like behavior in 1997, by Metzger[14].

LANDAUER MODEL

Shown in Figure 1.1 is a schematic of the electronic structure for a simple organic molecule such as benzenedithiol. For a short isolated molecule in vacuum, the Schrödinger equation can be used, along with an atomic potential model, to calculate the discrete allowed electronic energy levels and states (also called molecular orbitals). In its ground state energetic configuration, the highest-energy orbital that contains electrons is termed the highest occupied molecular orbital (HOMO). Above this state is the lowest unoccupied molecular orbital (LUMO). It will be seen later that these two orbitals play the most important role in determining the transport properties of the molecule.

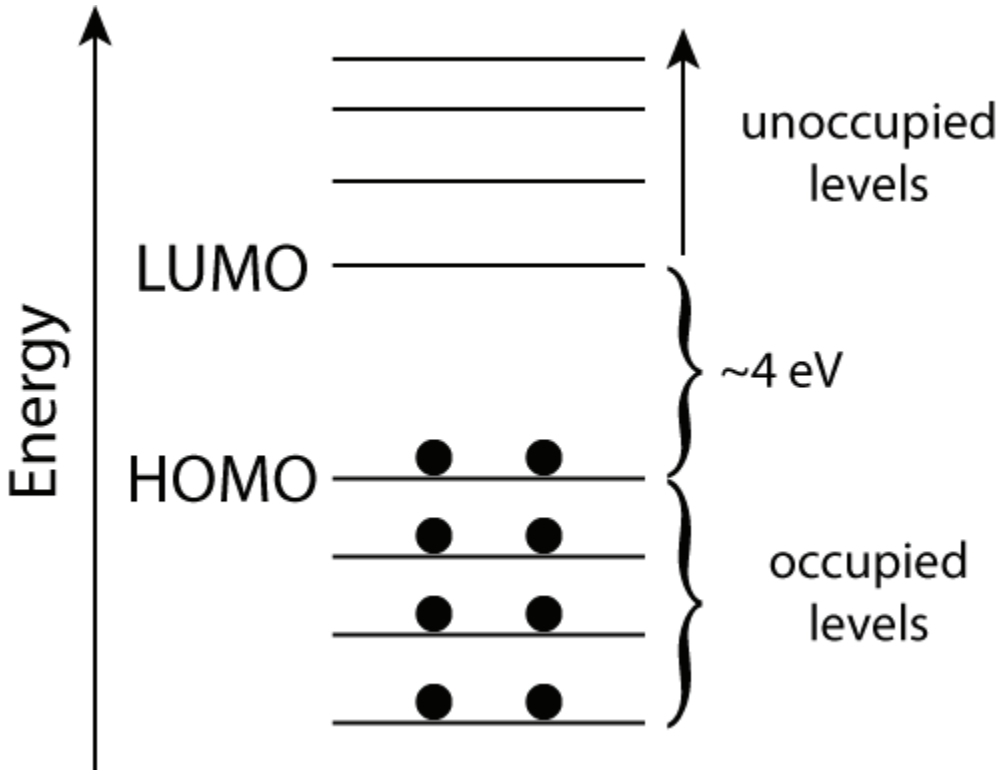

Figure 1.1 – Energy levels of a prototypical molecule (e.g. benzenedithiol) in vacuum.[15]

When the molecule is brought into weak contact with bulk electrodes which have a continuum of energy states, the molecular energy levels align energetically with the electrode such that at equilibrium, the chemical potential falls in between the HOMO and LUMO, as shown in Figure 1.2a. If a small bias is applied across the electrodes, the chemical potential will move with respect to the grounded electrode by eV:

$$\mu_1 - \mu_2 = eV$$

The Fermi distributions at any energy level at each electrode are

$$f_1 = f_1(E - \mu_1) = \frac{1}{1 + \exp[(E - \mu_1)/k_B T]}$$

$$f_2 = f_2(E - \mu_2) = \frac{1}{1 + \exp[(E - \mu_2)/k_B T]}$$

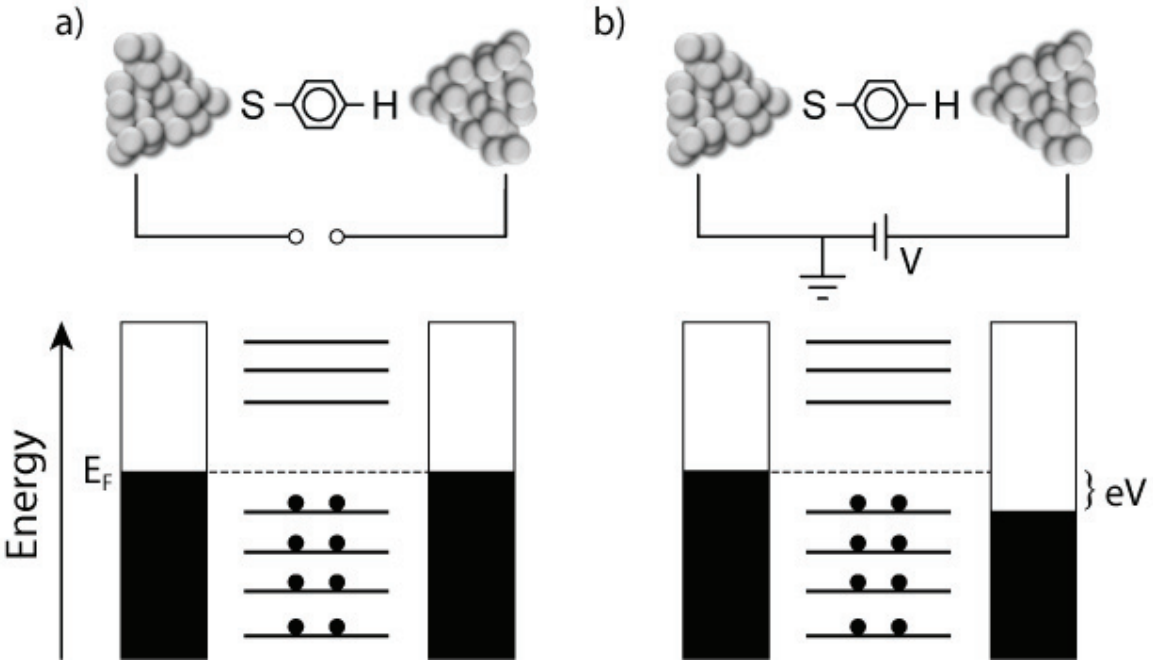

Figure 1.2 – Electronic structure of a weakly coupled metal-molecule-metal junction. a) open circuit electronic structure; b) applied voltage V.

As the applied potential is increased, chemical potential of one of the electrodes will cross one of the molecular orbitals (either the HOMO or LUMO; Figure 1.2b). Let us call the energy of this molecular orbital ε and consider the number of electrons that exist in the electrodes at equilibrium. The left electrode tries to maintain an average number of $2f_1(\varepsilon)$ electrons at this level, and will seeks to bring the molecule into equilibrium with itself by injecting electrons into it. At the same time, the right electrode tries to maintain $2f_2(\varepsilon)$ electrons at this level, and also tries to bring the molecule into equilibrium with itself by pulling electrons out. An average number of electrons, $n(\varepsilon)$, will exist, in the molecule at this energy level, where $n(\varepsilon)$ is somewhere between the $2f_1(\varepsilon)$ and $2f_2(\varepsilon)$. A non-equilibrium state is set up between the two electrodes that causes a current to flow through the junction.

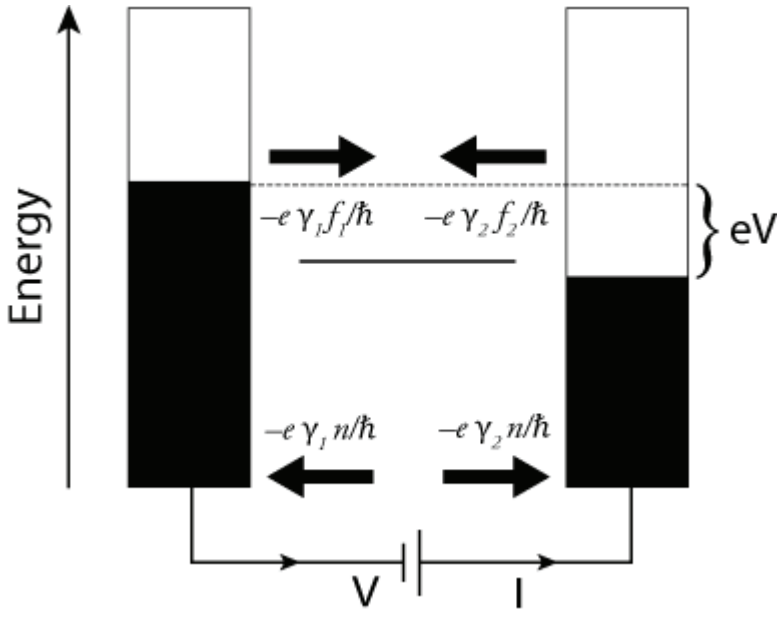

Figure 1.3 – Charge flow through a one-level molecular junction.

A simple relationship can be derived that expresses the current I in terms of the rates of electron transfer between molecule and electrode, as well as the chemical potentials of

the electrodes. This is diagrammatically demonstrated in Figure 1.3. Assuming that there is only one molecular level through which transport occurs, we can write the rate of transfer (s^{-1}) between the left and right electrodes as $\gamma_1/\hbar$ and $\gamma_2/\hbar$, respectively. The terms γ_i are a measure of how strongly coupled the molecule is to electrode i, and $\hbar$ is Planck's constant divided by 2π. The flow rate of charge from the left electrode to the molecule is a product of the charge on the carrier species (in this example, let us assume that electrons are the charge carrying species), the transfer rate and the average number of electrons present: $-e\gamma_1 f_1(\varepsilon)/\hbar$. Similarly, the rate of charge flow from the molecule to the left electrode is $-e\,\gamma_1 n(\varepsilon)/\hbar$. If we take electrons to be the charge carriers, we define the current to be opposite to the rate of charge flow:

$$I_1 = -(flow\ of\ electrons) = -\left[\frac{-e\gamma_1}{\hbar}2f_1(\varepsilon) - \frac{-e\gamma_1}{\hbar}n(\varepsilon)\right] = \frac{\gamma_1 e}{\hbar}\big(2f_1(\varepsilon) - n(\varepsilon)\big)$$

Similarly, for the junction between the molecule and the right electrode:

$$I_2 = -(flow\ of\ electrons) = -\left[\frac{-e\gamma_2}{\hbar}n(\varepsilon) - \frac{-e\gamma_2}{\hbar}2f_2(\varepsilon)\right] = \frac{\gamma_2 e}{\hbar}\big(n(\varepsilon) - 2f_2(\varepsilon)\big)$$

At steady state,

$$I_1 = I_2$$

We can derive an expression for the steady-state current, I, that is independent of the average number of carriers in the molecular orbital:

$$I = \frac{2e}{\hbar}\frac{\gamma_1\gamma_2}{\gamma_1 + \gamma_2}\big(f_1(\varepsilon) - f_2(\varepsilon)\big)$$

At 0 K, this expression simplifies to

$$I_{T=0K} = \frac{2e}{\hbar}\frac{\gamma_1\gamma_2}{\gamma_1 + \gamma_2}$$

According to this simple model, one could achieve an infinite amount of current simply by strongly coupling the molecule to the electrodes (i.e. increasing γ_1 and γ_2). This discrepancy arises because the assumption of a discrete molecular orbital level is only valid when the molecule is very weakly coupled to the electrodes. The density of states (DOS) of a weakly coupled electrode-molecule-electrode system can be represented by a delta function:

$$D(E) = \delta(E - \varepsilon)$$

When the molecule is more strongly coupled to the electrodes, the molecular orbital levels mix with the continuum of energy states in the electrodes and transform into a spread of energies, as shown in Figure 1.4. The broadened DOS can be expressed as a Lorentzian function centered around ε:

$$D(E) \approx \frac{(\gamma_1 + \gamma_2)/2\pi}{(E - \varepsilon)^2 + \left(\frac{\gamma_1 + \gamma_2}{2}\right)^2}$$

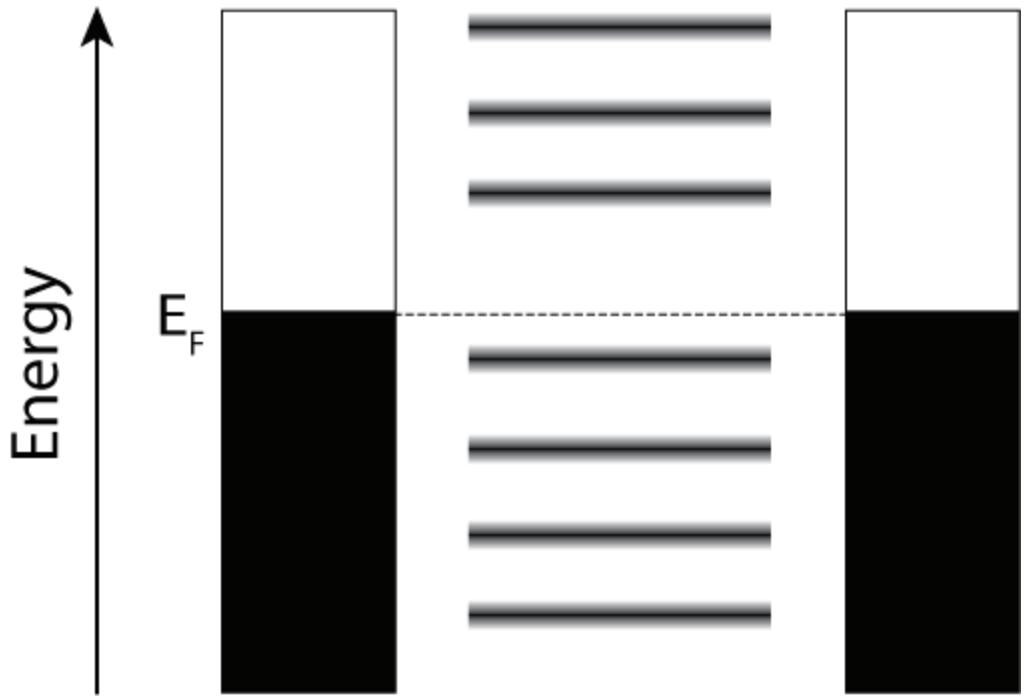

Figure 1.4 – Broadening in molecular energy levels as the result of strong coupling to the electrodes.

In the more general case (with the level broadening effect in mind), one needs to integrate over all energies to obtain the sum of contributions to current at various energies where transport can occur through the molecule. The new expression for the current flowing through the junction is

$$I = \frac{2e}{\hbar}\frac{\gamma_1\gamma_2}{\gamma_1+\gamma_2}\int_{-\infty}^{\infty} D(E)[f_1(E)-f_2(E)]dE$$

Substituting for $D(E)$,

$$I = \frac{2e}{\hbar}\frac{\gamma_1\gamma_2}{\gamma_1+\gamma_2}\int_{-\infty}^{\infty} \frac{(\gamma_1+\gamma_2)/2\pi}{(E-\varepsilon)^2+\left(\frac{\gamma_1+\gamma_2}{2}\right)^2}[f_1(E)-f_2(E)]dE$$

At low temperatures and small biases, we can write

$$f_1 - f_2 = eV\left(-\left.\frac{df(E)}{dE}\right|_{E=\varepsilon}\right) = eV\delta(E-\varepsilon)$$

Therefore,

$$I|_{\substack{low\ T,\\ small\ V}} = \frac{2e}{\hbar}\frac{\gamma_1\gamma_2}{\gamma_1+\gamma_2}\frac{(\gamma_1+\gamma_2)/2\pi}{\left(\frac{\gamma_1+\gamma_2}{2}\right)^2}eV$$

Making the assumption that the molecule is symmetrical and that the coupling energies to the electrodes are the same,

$$I|_{\substack{low\ T,\\ small\ V}} = \frac{2e}{\hbar}\frac{\gamma^2}{2\gamma}\frac{2\gamma/2\pi}{\gamma^2}eV = \frac{2e^2}{h}V$$

We can now write the conductance of a simple one-level electrode-molecule-electrode junction at low temperatures and small biases as

$$G_0 \equiv \left.\frac{I}{V}\right|_{\substack{low\ T,\\ small\ V}} = \frac{2e^2}{h} = \frac{1}{12.9\ k\Omega} = 0.775\ \Omega^{-1}$$

G_0 is often termed the quantum of electrical conductance. The broadening due to increased electrode-molecule coupling creates an upper bound for the value of G_0 for a perfectly conducting channel. Experimentally determined in 1988 by two independent groups[16,17] who measured the conductance of the quantum point contact created by a GaAs-AlGaAs heterojunction.

It is useful to define a term called the transmission, $T(E)$, of the junction:

$$T(E) = 2\pi D(E)\frac{\gamma_1\gamma_2}{\gamma_1 + \gamma_2}$$

We can now write the current as

$$I = \frac{2e}{h}\int_{-\infty}^{\infty} T(E)[f_1(E) - f_2(E)]dE$$

This is the Landauer formula[18-20], and will be used later to develop an expression for the thermopower of a metal-molecule-metal junction. Using a Lorentzian to model molecular orbitals is a good model when the density of states in the contact is constant and if the molecule is weakly coupled to the electrodes[21]. Though it has been derived with these assumptions in mind, it has still been shown to be a good approximation by recent computational papers[22-24].

If we evaluate the Landauer formula at low temperatures, a small bias, and a single molecular level through which electrons can be transported through, we can obtain a simple, intuitive formula:

$$I = \frac{2e^2}{h}T(\varepsilon)V; \qquad G = \frac{2e^2}{h}T(\varepsilon)$$

The transmission function at the molecular orbital energy level, $T(\varepsilon)$, is often approximated[15,25,26] as a tunneling barrier as

$$T(\varepsilon) = A\exp\left(-\frac{\sqrt{2m\alpha E_b}}{\hbar}L\right) = A\exp(-\beta L)$$

where A is a constant, m is the effective mass of the electron[25], $\hbar$ is Plank's constant divided by 2π, and L is the length of the molecule (or barrier width). α is a parameter that accounts for the symmetry in the potential profile across the electrode-molecule-electrode junction. For symmetric molecules (e.g. the aromatic dithiol molecules we will use in this work), α = 1. E_b is the barrier height:

$$E_b = \phi - (eV/2)$$

where V is the applied voltage, and ϕ is the distance of the closest molecular orbital level from the Fermi level at zero bias. We can thus write a simplified formula for the conductance of a non-ideal junction as

$$G = \frac{2e^2}{h}A\exp(-\beta L) = G_0\exp(-\beta L); \qquad R = R_0\exp(\beta L)$$

This exponential dependence of junction conductance and resistance on molecular length has been observed experimentally by several groups[15,26-30]. The value of the tunneling decay parameter, β, varies widely even among measurements of the same molecular junction. For alkanethiols, values from 0.6 to 1.3 Å have been reported. For aromatic thiols, which we study in this report, values from 0.1 to 0.6 Å have been observed[30].

THERMOELECTRICITY

If a temperature difference exists between two points in a conductor or semiconductor, a voltage difference results between these points. This is called the Seebeck effect, or the thermoelectric effect; in other words, a thermal gradient gives rise to a built-in electric

field. The Seebeck coefficient, or thermopower, relates the amount of potential difference developed in a material to an applied temperature differential:

$$S = -\frac{V_1 - V_2}{T_1 - T_2} = -\frac{\Delta V}{\Delta T}$$

One can also write the Seebeck coefficient as

$$\mathbf{E} = S\nabla T$$

where **E** is the electric field brought about by the temperature gradient.

Early thermocouples were metallic, but many more recently developed thermoelectric devices are made from alternating p-type and n-type semiconductor elements connected by metallic connectors. Semiconductor junctions are common in power generation devices, while metallic junctions are more common in temperature measurement. Charge flows through the n-type element, crosses a metallic interconnect, and passes into the p-type element. If a power source is provided, the thermoelectric device may act as a cooler by the Peltier effect (a current causes a temperature gradient across a material). Electrons in the n-type element move opposite the direction of current and holes in the p-type element will move in the direction of current, both removing heat from one side of the device. When a temperature difference is set up across a material the thermoelectric device functions as a power generator. The heat source drives electrons in the n-type element toward the cooler region, creating a current through the circuit. Holes in the p-type element then flow in the direction of the current. Therefore, thermal energy is converted into electrical energy.

Microscopically, one can attribute the thermoelectric effect to two phenomena: charge carrier diffusion and phonon drag (the latter only becoming pronounced at low temperatures). Electrons and holes, depending on the material, have different thermal energies in different parts of a material when it is at a non-uniform temperature, and there will be a resultant net flux. The average energy per electron in a metal, E_{av}, with a 3D density of states $g(E) \propto E^{1/2}$ is given by

$$E_{av}(T) = \frac{3}{5} E_{F0} \left[1 + \frac{5\pi^2}{12} \left(\frac{kT}{E_{F0}} \right)^2 \right]$$

where E_{F0} is the Fermi energy, k is Boltzmann's constant, and T is the temperature[31,32]. It is clear from the above equation that the energy of electrons in a hotter region will be higher. More energetic carriers in the hotter regions will diffuse to the colder regions. As thermal energy in the form of hot charge carriers is transported from one end to the other in the form of a heat current, a flow of charge accompanies it, creating a potential difference which prevents further diffusion if the material is in an open circuit.

Let us examine the potential dV that develops from a small temperature difference dT. Each electron that moves from the hot region to the cold region must do work to overcome this potential. In other words, it loses an amount of energy $-edV$ as it traverses the temperature difference. This amount of work can be expressed as

$$-edV = E_{av}(T + dT) - E_{av}(T)$$

Substituting from above and expanding $E_{av}(T + dT)$ by a Taylor series to the first order, we obtain

$$edV \approx -\frac{\pi^2 k^2 T dT}{2E_{F0}}$$

Therefore, for metals,

$$S \approx \frac{dV}{dT} = \frac{\pi^2 k^2 T}{2eE_{F0}}$$

However, both positive and negative Seebeck coefficients have been observed for metals. To reconcile this with the above equation, one must take into account not only the diffusion of electrons from hot to cold, but also the scattering of these electrons by impurities, imperfections, and lattice vibrations or phonons. The thermopower of a material is a collection of many different effects.

Let us define an adjacent hot and cold region, as shown in Figure 1.5. The width of the hot region is λ, the mean free path (MFP) along *x* in the hot region; the width of the cold region is λ', the MFP in the cold region. We can further define the electron densities in the hot and cold regions as *n* and *n*'. If the mean scattering time of electrons is τ , then the flux of electrons in the hot region moving towards the cold region is (*n* λ)/2τ. The net flux (accounting also for the movement of electrons from the cold region to the hot region) is

$$J = \frac{n\lambda}{2\tau} - \frac{n'\lambda'}{2\tau'}$$

Defining Δx to be λ, we can approximate the terms in the cold region as

$$n' = n + (dn/dx)\Delta x$$

$$\lambda' = \lambda + (d\lambda/dx)\Delta x$$

$$\tau' = \tau + (d\tau/dx)\Delta x$$

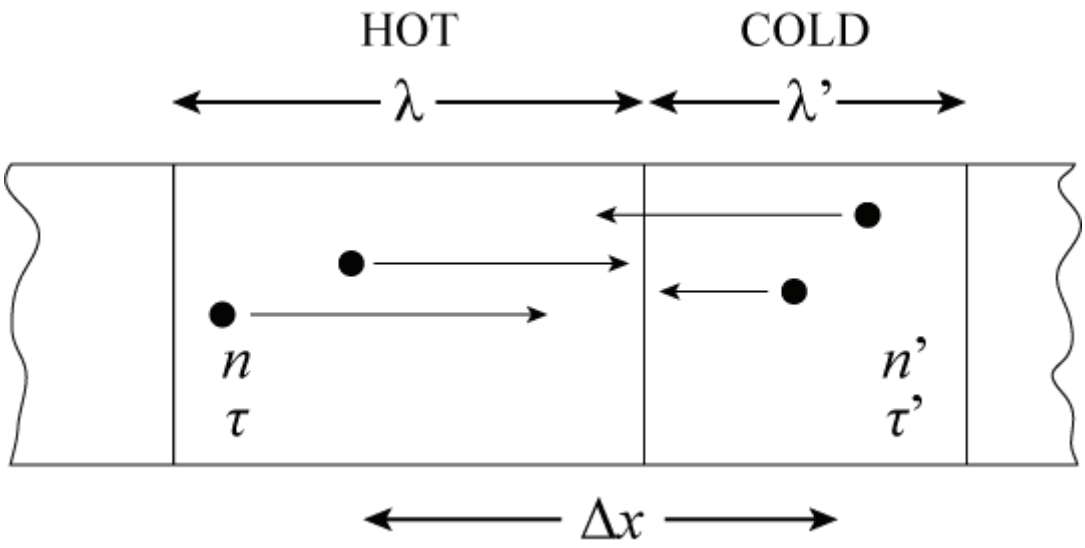

Figure 1.5 – Electron flow in adjacent hot and cold regions of a material. The widths of the two regions correspond to the mean free paths in each region. Half the electrons in each region will move in the +x direction, and half will move in the –x direction. The electrons in the hot region have higher energies on average than those in the cold region.[31]

The net flux is then

$$J = -\frac{\lambda^2}{2\tau}\left(\frac{\partial n}{\partial x}\right) - \frac{n\lambda}{2\tau}\left(\frac{\partial \lambda}{\partial x}\right) + \frac{n\lambda^2}{2\tau^2}\left(\frac{\partial \tau}{\partial x}\right)$$

$$= -\frac{\lambda^2}{2\tau}\left(\frac{\partial n}{\partial x}\right) - \frac{n\lambda}{2\tau}\left(\frac{\partial \lambda}{\partial x}\right) + \frac{n\lambda^2}{2\tau}\left(\frac{\partial \ln\tau}{\partial x}\right)$$

From this equation, it is clear that the carrier concentration, mean free path, and scaterring time all play a factor in determining whether the net flux results in an excess of electrons on the hot or cold side.

MOLECULAR THERMOELECTRICITY USING THE LANDAUER MODEL

If the transmission of a channel is not constant, inspection of the Landauer equation yields a finite current for a temperature difference in the two electrodes, even in the absence of any applied bias. If a temperature gradient was applied across the junction

and the electrodes were left in an open circuit configuration, one could measure the voltage developed across the junction. The Landauer equation can be used to derive an expression for the thermopower of a metal-molecule-metal junction in terms of the transmission of the channel, $T(E)$. This relationship was first developed by Butcher[33]. We derive it here using a differential approach: one electrode is heated slightly by an amount ΔT, which subsequently causes a small change in the chemical potential of the heated electrode ($\Delta\mu$) and a potential across the junction, V. The Fermi function of the heated electrode, f_2, can be expanded with respect to f_1:

$$f_2(E, \mu_2, T_2) = f_1(E, \mu_1 + \Delta\mu, T_2 + \Delta\mathrm{T})$$

$$\cong f_1(E, \mu_1, T_1) + \frac{\partial f_1}{\partial \mu_1}\Delta\mu + \frac{\partial f_1}{\partial T_1}\Delta T_1$$

Therefore,

$$f_1 - f_2 = -\left(\frac{\partial f_1}{\partial \mu_1}\Delta\mu + \frac{\partial f_1}{\partial T_1}\Delta T_1\right)$$

We express all partial derivatives of the Fermi function in terms of $\partial f / \partial E$:

$$\frac{\partial f_1}{\partial E} = -\frac{1}{k_B T_1}\frac{\exp[(E-\mu_1)/k_B T_1]}{\left[1+\exp[(E-\mu_1)/k_B T_1]\right]^2}$$

$$\frac{\partial f_1}{\partial \mu_1} = -\frac{\partial f_1}{\partial E} = \delta(E-\mu_1)$$

$$\frac{\partial f_1}{\partial T_1} = -\frac{E-\mu_1}{T_1}\frac{\partial f_1}{\partial E}$$

Therefore,

$$f_1 - f_2 = \frac{E-\mu_1}{T_1}\frac{\partial f_1}{\partial E}\Delta T_1 - \delta(E-\mu_1)\Delta\mu$$

Substituting this result into the integrand of the Landauer equation and specifying an open-current configuration, we obtain

$$I_{open} = 0 = -\frac{2e}{h}\int_{-\infty}^{\infty} T(E)\left(\frac{E-\mu_1}{T_1}\frac{\partial f_1}{\partial E}\Delta T_1 - \delta(E-\mu_1)\Delta\mu\right)dE$$

$$0 = -\frac{2e}{h}\int_{-\infty}^{\infty} T(E)\left(\frac{E-\mu_1}{T_1}\frac{\partial f_1}{\partial E}\Delta T_1\right)dE + \frac{2e}{h}T(\mu_1)\Delta\mu$$

$$\frac{\Delta\mu}{\Delta T_1} = \frac{1}{T(\mu_1)}\int_{-\infty}^{\infty} T(E)\left(\frac{E-\mu_1}{T_1}\frac{\partial f_1}{\partial E}\right)dE$$

We can also expand $T(E)$ in a Taylor series around the chemical potential of the cool electrode:

$$T(E) \cong T(\mu_1) + \left.\frac{\partial T(E)}{\partial E}\right|_{E=\mu_1}(E-\mu_1)$$

$$\frac{\Delta\mu}{\Delta T_1} = \frac{1}{T(\mu_1)}\int_{-\infty}^{\infty}\left[T(\mu_1) + \left.\frac{\partial T(E)}{\partial E}\right|_{E=\mu_1}(E-\mu_1)\right]\left(\frac{E-\mu_1}{T_1}\frac{\partial f_1}{\partial E}\right)dE$$

$$= \int_{-\infty}^{\infty}\left(\frac{E-\mu_1}{T_1}\frac{\partial f_1}{\partial E}\right)dE + \frac{1}{T(\mu_1)}\left.\frac{\partial T(E)}{\partial E}\right|_{E=\mu_1}\int_{-\infty}^{\infty}\frac{(E-\mu_1)^2}{T_1}\frac{\partial f_1}{\partial E}dE$$

The first integral evaluates to zero due to symmetry. The second integral can be evaluated by using the Sommerfeld expansion[34]:

$$\int_{-\infty}^{\infty}\frac{(E-\mu_1)^2}{T_1}\frac{\partial f_1}{\partial E}dE = -\frac{\pi^2 k_B^2 T_1}{3}$$

Therefore,

$$\frac{\Delta\mu}{\Delta T_1} = \frac{-\mathrm{eV}}{\Delta T_1} = -\frac{1}{T(\mu_1)}\left.\frac{\partial T(E)}{\partial E}\right|_{E=\mu_1}\frac{\pi^2 k_B^2 T_1}{3}$$

$$S = \frac{-V}{\Delta T_1} = -\frac{\pi^2 k_B^2 T_1}{3e} \frac{\partial \ln T(E)}{\partial E}\bigg|_{E=\mu_1}$$

We now have an equation that relates the thermopower to the transmission function of the junction. The greater the change in the transmission at the chemical potential, the greater the magnitude of the thermopower will be.

TRANSITION VOLTAGE SPECTROSCOPY

Transition voltage spectroscopy has recently been a popular tool in the molecular electronics community for analyzing the electrical characteristics of MMMJ's to gain information about their electronic structure. The analysis technique was developed by Beebe in 2006[35,36], and was based on the work by Simmons[37] on modeling the current-voltage characteristics of metal-insulator-metal junctions as a tunnel barrier:

$$I = \frac{eA}{4\pi^2 \hbar d^2}\left\{\left(\phi - \frac{eV}{2}\right)\exp\left(-\frac{2d\sqrt{2m_e}}{\hbar}\right)\sqrt{\phi - \frac{eV}{2}} - \left(\phi + \frac{eV}{2}\right)\exp\left(-\frac{2d\sqrt{2m_e}}{\hbar}\right)\sqrt{\phi + \frac{eV}{2}}\right\}$$

where e is the charge of a proton, A is the cross-sectional area of the junction, d is the barrier width, m_e is the effective mass of an electron, ϕ is the barrier height, and V is the applied voltage. While the barrier width in Simmons' work was considered to be the thickness of the insulating thin film, Beebe applied this equation to the scenario of a molecular junction, assuming that the barrier width corresponds to the length of the molecule. He also took the barrier height to be approximated by the energy offset between the electrode Fermi level and the nearest molecular orbital.

Simmons assumed that the potential profile would drop linearly across the insulator, and this was also the model that Beebe used for metal-molecule-metal junctions. At zero bias, the potential profile in this model would be analogous to a rectangular barrier that electrons at the electrode would have to tunnel through in order to reach the other electrode. At biases below that of the barrier height, the barrier would be trapezoidal in shape (the difference between the potential of the barrier and the Fermi level of either electrode is held constant). This corresponds to a charge transport mechanisms called direct (nonresonant) tunneling. As the bias exceeds the tunneling barrier height, the barrier becomes triangular in shape, and the effective barrier width begins to decrease with increasing bias – a scenario termed field emission, direct tunneling, or Fowler-Nordheim tunneling.

By plotting $\ln(I/V^2)$ versus the inverse voltage (V^{-1}), Beebe obtained plots that exhibited a minimum point, which he termed the transition voltage, V_{trans}. He argued that this transition voltage marked the transition from a rectangular/trapezoidal barrier shape (direct tunneling, low bias) to a triangular shape (field emission, high bias), and that one could experimentally estimate the barrier height associated with the molecule.

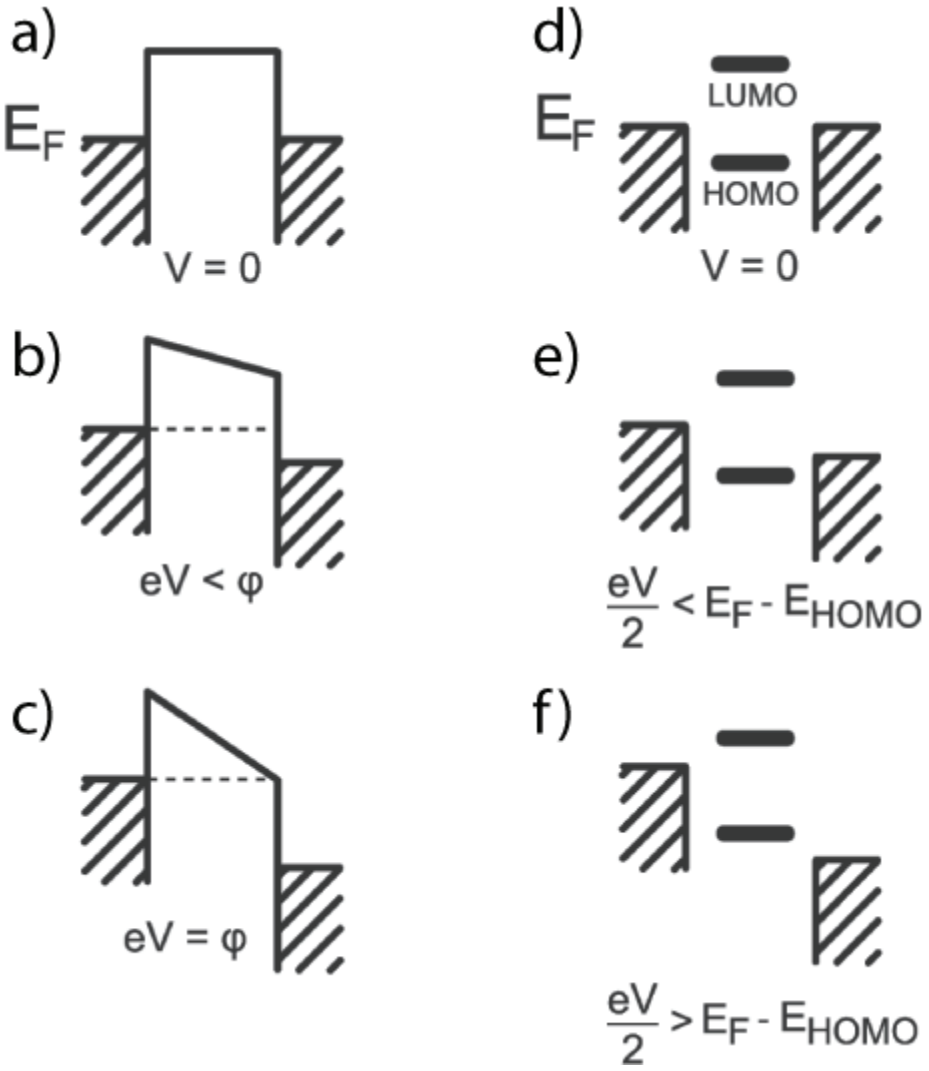

Figure 1.6 – Comparison of the two models used in describing electronic transport through a molecular junction. (a–c) Simmons model, where the molecule is depicted as a tunneling barrier. a) At no applied bias, the barrier is rectangular. b) When a bias is applied, the barrier is tilted and becomes trapezoidal. c) When the applied voltage exceeds the barrier height, the barrier becomes triangular and tunneling occurs by field emission. (d-f) Landauer model. d) Discrete molecular orbitals are broadened by coupling to the electrodes. e) For an applied bias, transport is allowed in the energy range of size eV between the chemical potential of the left and right electrodes. f) At high biases, when one of the molecular levels crosses crosses into the bias window, resonant tunneling occurs, and there is a large increase in current.[38]

More recently, other groups have questioned the use of the Simmons model and thinking of the molecule as a tunneling barrier to electron transport. In 2009, Huisman

demonstrated computationally that the Simmons model was actually inconsistent with experimental data[38]. Instead, a coherent transport model, where the molecule is represented by molecular orbitals with Lorentzian transmission functions, agrees well with the experimental data. In this picture, the transition voltage could be used as an estimate of the distance of the Fermi level to the nearest molecular orbital.

In 2010, the effect of molecule symmetry/asymmetry on TVS was computationally studied by Chen et al.[39] using an ab initio approach and density functional theory combined with a nonequilibrium Green's function method. They found that relating V_{trans} to the energetic separation between the Fermi level and the closest molecular orbital (in their case, the HOMO) was most accurate when the chemical structure of the molecule was symmetric. A subsequent paper[23] in 2011 by the same group investigated the possibilities of analyzing current-voltage data by plotting $\ln(I/V^a)$ versus $1/V$, where $a < 2$. They showed that the voltage required to determine the energetic position of the molecular levels could be reduced by about 30% compared to conventional TVS analyses.

Other computational studies have taken the electrostatic potential profile[6,40] of the molecule into account to ascertain the appropriateness of using TVS in molecular systems[41,42]. The potential profile depends largely on the screening from π electrons of an applied voltage. For conjugated (aromatic) molecules, the screening is large, and the voltage drop occurs mostly at the contacts. For non-conjugated (aliphatic) molecules, there is little screening, and there is a linear decrease in the potential throughout the length of the molecule. In addition, aliphatic molecules are known to have a much larger HOMO-LUMO gap (~8 eV) than aromatic molecules (~4-5 eV)[15]. The degree of

screening has been related to the HOMO-LUMO gap: strong screening results in a small HOMO-LUMO gap. Mirjani[41] calculated the TVS response versus the HOMO-Fermi level separation for a series of junctions bridged by a row of quantum dots, and found that there was only a strong correlation between the two for molecules with no potential drop across the junction (strong screening). This suggests that TVS can only be reliable tool for estimating the energetic position of the frontier orbitals for molecules exhibiting strong screening, such as conjugated systems.

ORGANIZATION OF THE THESIS

This thesis will present our findings on the electrical and thermoelectric properties of metal-molecule-metal junctions.

Chapter 2 will present an overview of past methods for measuring electrical properties and thermoelectric properties of molecular junctions. It will conclude with a description of new the atomic force microscope based experimental technique we developed that allows for the concurrent measurement of both the electrical and thermoelectric properties of a small number of molecules self-assembled on a conductive surface.

Chapter 3 will present our findings on the electrical characteristics of several aromatic molecular junctions. The low-bias conductance of these molecules will be presented, and the effect of length and contact coupling strength will be examined. Furthermore, an analysis of this data using transition voltage spectroscopy will be performed for a series of aromatic monothiol molecular junctions to obtain an approximation of the energetic separation of the electrodes' Fermi level to the closest molecular orbital.

Chapter 4 will describe the new atomic force microscope-based technique developed by us to measure the thermopower of metal-molecule-metal junctions. We investigate the

effect of contact coupling strength and contact chemistry on the thermoelectric properties of the junction. Using the expression for the Seebeck coefficient of MMMJ's obtained using the Landauer model, we will relate the sign of the junction Seebeck coefficient to the electronic structure of the MMMJ's. We will interpret our results to determine conclusively whether the HOMO or LUMO is closer to the electrodes' chemical potential, and specifically demonstrate an example of how molecular structure can be altered (i.e. by changing the endgroup from thiol to isocyanide) to effect a change from HOMO- to LUMO-dominated transport.

Chapter 5 will conclude this work with suggestions of how to further advance this work and better understand the electronic structure of molecular junctions.

Chapter 2

Experimental Apparatus

Past Experimental Methods to Measure Electrical and Thermoelectric Properties of Molecular Junctions

Right before and around the turn of the century, a number of ingenious experimental techniques were devised to probe and study the electrical properties of organic molecular junctions.[26,43-45]. The primary achievement of these apparatuses is to trap one or a small number of molecules between two conducting electrodes for a long enough time that electrical measurements can be performed. These experiments provide important insights into many molecular transport phenomena like quantized charge transport[43], negative differential resistance[46], Coulomb blockade[47], and rectification[48]. There are always questions as to whether the data obtained from these devices are the result of impurities or defects in the systems, rather than by the molecular species under study, so each device must undergo much scrutiny and careful characterization and analysis if is to become accepted as a reliable tool for molecular electronics experiments[49]. Presented in this chapter is a survey of the landmark developments in experimental techniques that have enabled the field of molecular electronics to progress from theory into physical realization. The chapter will conclude with a description of the new experimental

technique developed by us to measure the thermopower of molecular junctions using an AFM-based setup.

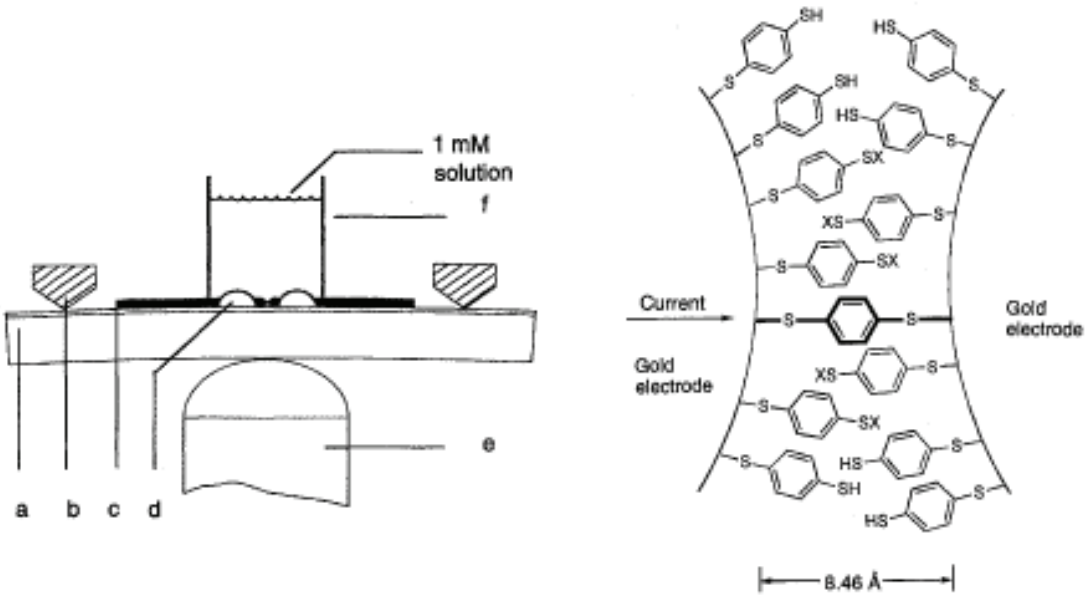

Figure 2.1 – Schematic of a mechanically controllable break junction[50]. a) the apparatus; b) a self-assembled monolayer of benzenedithiol molecules formed between the gap.

One of the first works demonstrating the trapping and characterization of a molecule between two electrodes was in 1997, by Reed and Tour[50]. As shown in Figure 2.1, their apparatus – called a mechanically controllable break junction (MCBJ) – consisted of a thin wire with a notch on it, which is glued onto a flexible substrate. The wire is fractured when the substrate is bent by a piezoelectric tube underneath it, allowing for an adjustable tunneling gap at the fracture point, and for molecules to assemble in between the gap when the apparatus is immersed in a solution containing the molecules. The large reduction factor between the gap distance and the motion of the piezoelectric tube allows for sub-angstrom control of the gap. The conductance of benzene-1,4-dithiolate self assembled monolayers were measured using large bias sweeps (–5 V to +5 V). While

these MCBJs were eventually found to be difficult to characterize and unwieldy due to frequent short circuiting, they opened up a new field of single-molecule electronics.

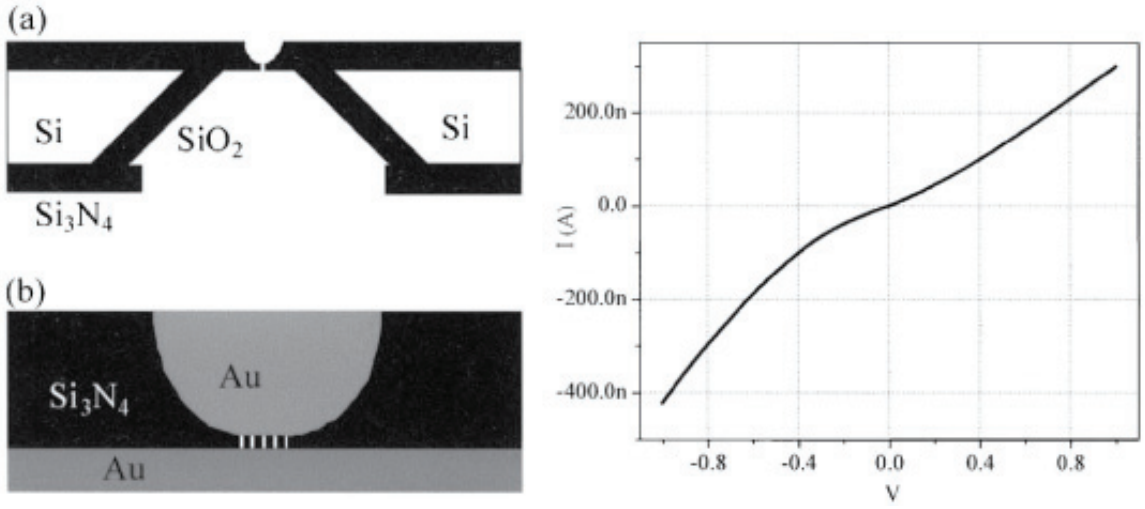

Figure 2.2 – Schematic of a nanopore junction formed from a suspended silicon nitride (Si_3N_4) membrane, and I-V characteristics of a 1,4-phenylene diisocyanide junction sandwiched in the pore between two gold electrodes[51].

In the same year, Reed and Tour developed a microfabricated apparatus containing a nanopore, depicted in Figure 2.2[46,51,52]. The device consisted of a self-assembled monolayer at the nanopore sandwiched between a top and bottom metallic contact[46,52]. In this configuration, a small ensemble of molecules is measured. The electrical properties of the molecules are assumed to behave in a non-interacting, parallel configuration. It was crucial that the SAM-electrode interface be reproducible. The nanopore geometry was first used to investigate the dependence of the conduction characteristics of a conjugated molecule with temperature. It was prone to having pin-holes through the nanopore monolayer that short circuited the top and bottom metal films.

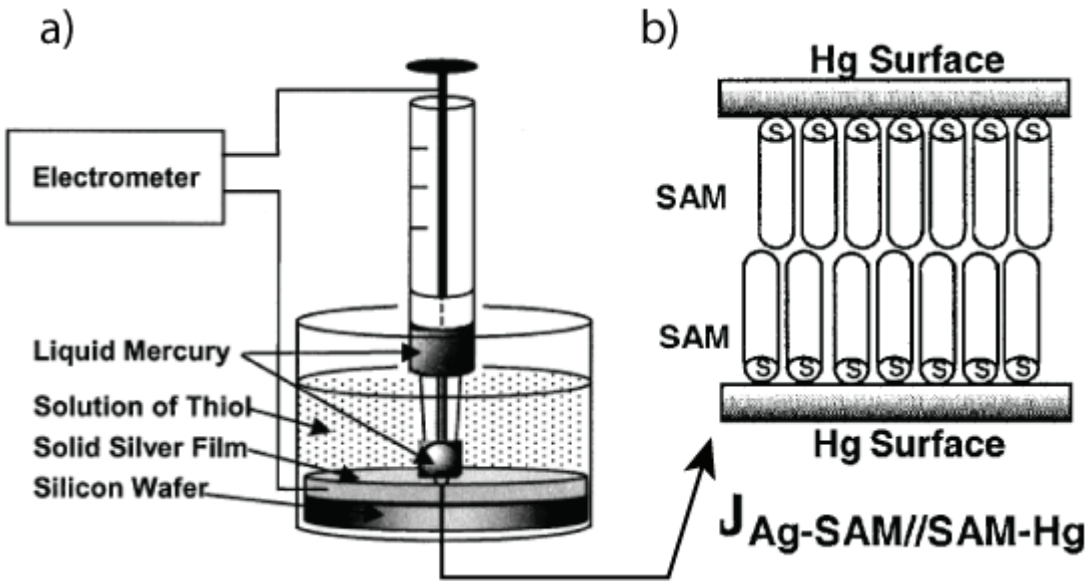

Figure 2.3 – Schematic of a mercury drop junction. a) the apparatus; b) diagram of the self-assembled bilayer sandwiched between two mercury electrodes.

The next experimental development involved having a more compliant top electrode instead of a rigid deposited thin film[53-55]. They made two SAMs which were composed of different or identical molecules: one monolayer was deposited on a flat silver substrate and the other on the surface of a small mercury droplet. Silver and mercury served as the electrodes, and the surface coatings were brought together in the geometry shown in Figure 2.3. Several results have been achieved through this method, including conductivity measurements[53,55].

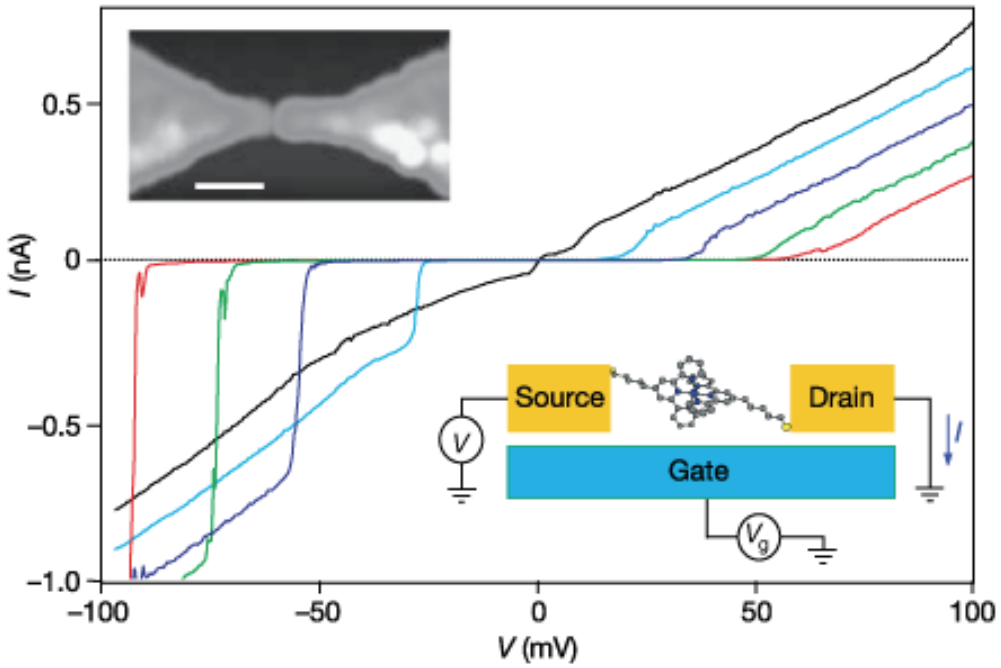

Figure 2.4 – Schematic of an electromigrated break junction[56]. The 1-2 nm wide gap holds a cobalt-centered polypyridyl ring. The current-voltage characteristics demonstrate the Kondo effect attached by thiol-terminated chains, and are obtained at low temperatures (100 mK).

Electromigration techniques are similar to the MCBJ setup in that a small gap is created at a fracture point to trap molecules in between it. With electromigrated break junctions (EBJ), the fracture is the result of sending a large current through a very narrow junction in a wire[47,56]. When optimized, this can result in a nanometer-sized gap that is buffered on either side by two stable contacts (Figure 2.4). A particular merit of this setup is the ability to have 3-terminal configurations in such devices, making this an ideal candidate for the construction of molecular transistors. A gate electrode can easily be microfabricated underneath the narrow region of the wire where the fracture is expected to occur. In 2002, Park and Ralph developed this technique and demonstrated Coulomb blockade and the Kondo effect on a "single-molecule transistor" using a cobalt-center

organometallic complex[56]. While making available unique parameters such as 3-terminal gating that are not readily possible with other techniques, the low yield of EBJs presents a challenge towards using this technique.

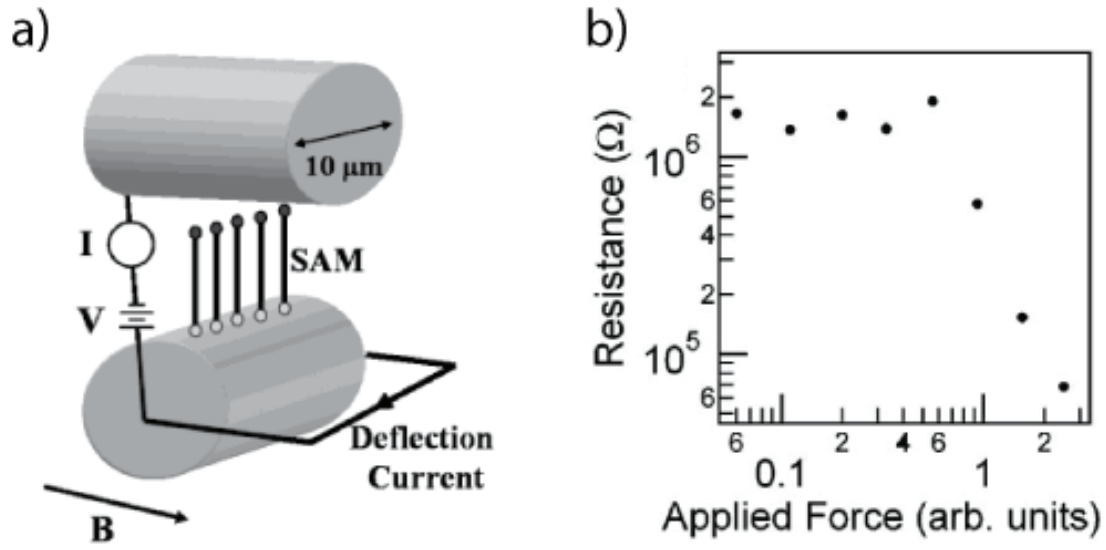

Figure 2.5 – Schematic of the crossed wire technique[57,58]. a) the apparatus; b) low-bias resistance measurements for various contact forces, controlled by the strength of the applied magnetic field.

The crossed wire technique was first employed by Kushmerick to form molecular junctions[57-59], and involves bringing two perpendicular metallic wires into contact with each other, shown in Figure 2.5. Movement of the wires is controlled by passing a small dc current through the wires under the presence of a magnetic field. One of the two wires is coated with an organic monolayer, and a MMMJ is formed at the contact point between the two wires. The estimated number of molecules in the junction is about 1000.

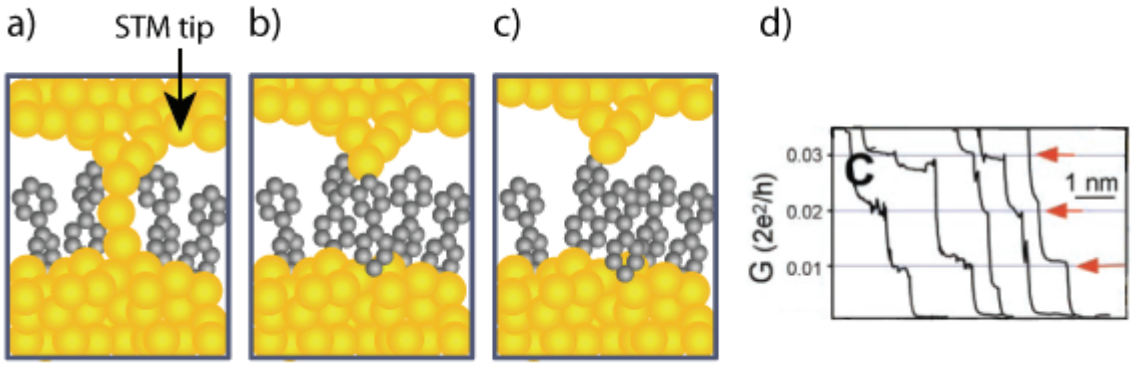

Figure 2.6 – Schematic of an STMBJ and the technique used to form single molecule junctions. a) the STM tip is brought into contact with the gold substrate, and then slowly withdrawn. Several molecules near the gold point contact will have bound to the tip. b) as the tip is withdrawn, molecules will begin to break off from the tip one by one. c) eventually, only one molecule will remain which forms a junction between the gold tip and substrate. d) multiple I-V curves of the STMBJ as the tip is being withdrawn. Steps showing multiples of the single-molecule conductance value are seen, suggesting the sequential breaking of molecular junctions.

Perhaps the most versatile and instructive class of techniques used in molecular electronics are those based on scanning probes. These primarily hinge on the innovations of Binnig and Rohrer in 1982[60] (scanning tunneling microscope) and just a few years later, Binnig and Quate in 1986[61] (atomic force microscope). The latter will be discussed in the next section, as it is most relevant to the current work.

The first instance of a STM used to measure molecular electronic transport was in 1996[62]. Tour and Bumm used STM to measure the conductance of conjugated thioacetate molecules dispersed in a SAM of poor-conducting aliphatic thiols, all assembled onto a gold surface. A later experiment by Xu and Tao in 2003[43] removed the need to embed a molecule of interest among a monolayer of other molecules. Their technique, shown in Figure 2.6, has indeed become the standard practice used for STM based molecular electronic experiments[63], and displays an unambiguous identification of single molecule

electronic conductance by the observation of quantized steps in I-V plots. The method also allows for statistical analysis of data: thousands of junctions can be easily made, broken, and reformed in a matter of minutes. The approach was to have the gold STM tip penetrate through a monolayer-coated surface and crash into the metallic surface (in their case, gold). In many cases, a few molecules will bind to the sides of the tip during this time. Once the control system registers that the conductance has exceeded a certain value, it begins retracting the STM tip away from the substrate surface. At first, quantized steps of height G_0 are observed, indicative of gold tip-substrate bonds being broken one by one. As the final gold chain breaks and the conductance drops below G_0, much smaller-sized steps were observed. Control experiments were performed to show that these small steps were due to the presence of molecules on the surface. The last and smallest of these steps was taken to be the single molecule conductance.

Apparatus Used for Measurement of Electrical Conductance and Thermopower

Here, we describe a simple AFM-based technique that enables, at room temperature and ambient conditions, concurrent measurement of both the electrical and thermoelectric response of a molecular junction. This is achieved by trapping organic molecules between a metal substrate and a metal-coated atomic force microscope tip.

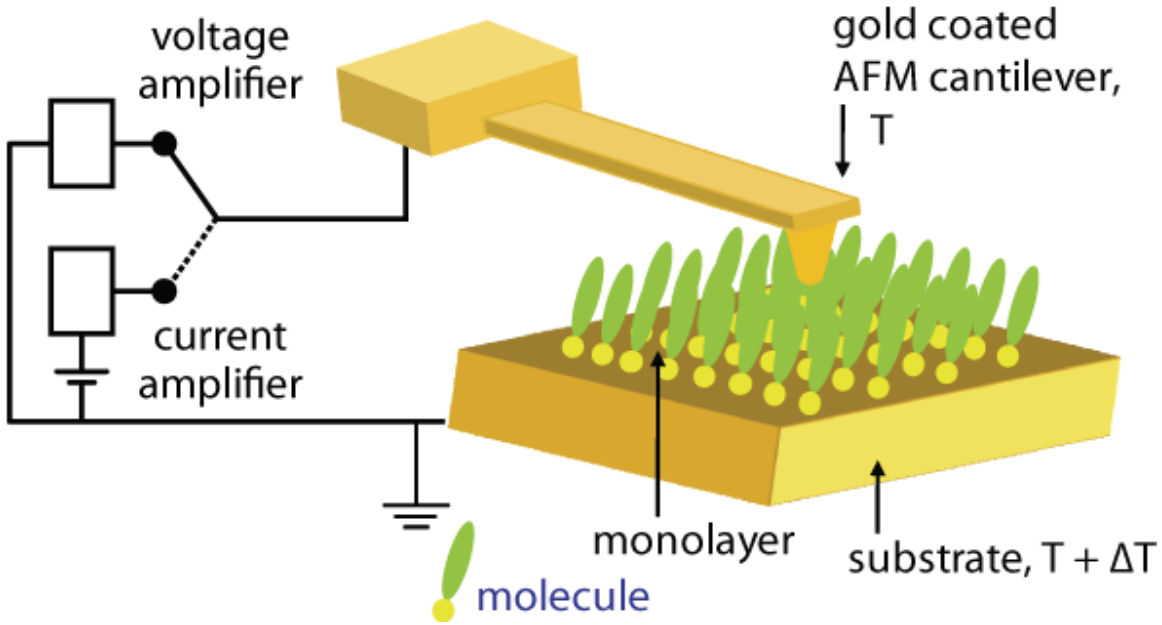

Figure 2.7 – Schematic of an AFM-based experimental setup for measurement of the electrical conductance and thermoelectric properties of molecular junctions[64].

Figure 2.7 shows a schematic illustrating a MMMJ created by placing a Au-coated AFM cantilever in soft mechanical contact (~1 nN contact force) with a Au substrate covered with a self-assembled monolayer of molecules, thus creating a molecular junction with multiple molecules[27-30,35,59] (~100) trapped in it. In fact, this technique for creating molecular junctions, called conducting probe atomic force microscopy (CP-AFM), was originally pioneered by Wold and Frisbie[28] and has been used extensively to characterize the electrical conductance and current-voltage characteristics of MMMJs. The commercial AFM system used in this work was the 5500 model, produced by Agilent Technologies. The molecules studied in this work are shown in Figure 2.8.

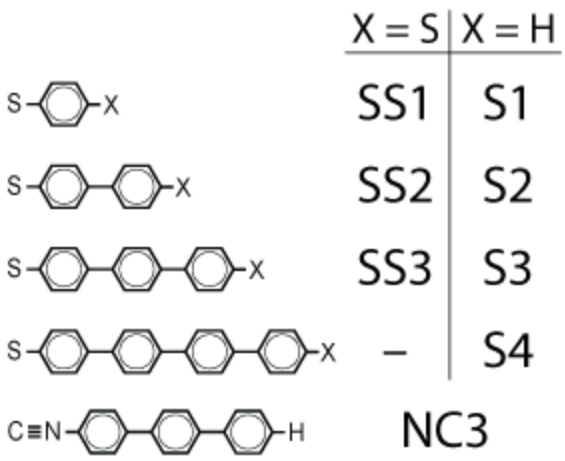

Figure 2.8 – Aromatic molecules used in this work. Monothiols are labeled S1, S2, S3, and S4; dithiols are labeled SS1, SS2, and SS3; the three-ringed isocyanide molecule is labeled NC3.

In our experiment we make two important additions to the commercial instrumentation in order to generate thermal gradients across the metal-molecule-metal junction for thermopower measurements: 1) an electrical heater is used to heat the substrate to an elevated temperature $T+\Delta T$ and, 2) a short (~ 125 μm long, 35 μm wide, and 1 μm thick) silicon cantilever coated with gold (instead of a silicon nitride cantilever traditionally employed in CP-AFM) is chosen and anchored to a thermal reservoir at a temperature T.

A square-inch adhesive strip heater (Omega) was attached to the underside of a custom-made sample plate, whose centre is made of a cylinder of Invar suspended by screws (for thermal isolation) to the main plate. The gold substrates were clamped to the top of the Invar cylinder. Temperature calibrations were performed by placing one thermocouple on the substrate surface and another on the body of the silicon cantilever. Given the large thermal conductivity of silicon[65] (~150 W/m·K) and the relatively poor thermal conductivity of the surrounding air (~0.024 W/m·K), our thermal modeling (see Appendix 1) suggests that the temperature of the metal-coated cantilever tip which is in contact with molecules must be between T and $T + 0.05\Delta T$. This implies that at least 95%

of the temperature differential (ΔT) occurs across the molecules trapped in between the metal electrodes (this thermal model was first introduced by Shi and Majumdar[66]; they verified this model by performing experiments with AFM cantilevers that have microfabricated thermocouples positioned at their tips).

The thermoelectric voltage of the junction is measured by a custom-built voltage amplifier with an input impedance of over 100 MΩ. The potential is measured between the gold-coated AFM cantilever and the gold-coated substrate (Figure 2.7). Aside from the temperature drop across the molecule, there is also a temperature drop in the copper wire between the gold substrate and the voltage amplifier lead. This affects the thermoelectric voltage measured by the amplifier, and will be discussed in detail in Chapter 4. An electronic relay circuit was built to allow fast switching between the current and voltage amplifier for concurrent electrical and thermopower measurements.

Chapter 3

Electrical Characteristics of Molecular Junctions

In this chapter, we present our findings on the response of various metal-molecule-metal junctions to an applied bias. In the first part, we will investigate the effect of molecular length and contact coupling strength on the resistance of junctions. Afterwards, we employ the TVS technique to garner an estimate of the energetic separation between the closest molecular orbital and the Fermi level of the electrodes for a series of molecules with sequentially increasing molecular length.

In order to characterize electrical transport in junctions the AFM tip was grounded while a bias voltage was applied to the substrate (Figure 2.7). A low-noise SRS 570 current amplifier was used to monitor the electrical current during these measurements. A custom LabVIEW program was written to automatically sweep the applied potential.

Effect of Molecular Length and Contact Coupling Strength on the Resistance of a Junction

I-V curves were obtained for molecular junctions formed from aromatic monothiol and dithiol monolayers shown in Figure 2.8. The data used for calculating junction conductance was obtained using only freshly coated AFM tips (see Appendix 3) to ensure a minimal variation in the tip diameter. After coating the tips the average radius was approximately 75 nm; each tip was inspected using a high-resolution SEM to ensure

uniformity of the radius. The contact area for such a tip can be estimated by using Hertzian mechanics[67]. First, the contact radius can be expressed as:

$$a = \left(\frac{RF_{\text{applied}}}{K}\right)^{1/3}$$

Where R is the radius of the tip, F_{applied} is the applied load on the junction, and K is the modulus of elasticity of the surface (77 GPa for gold, assuming that the monolayer's modulus is very low compared to that of the bulk gold layer underneath). The contact area is then

$$A = \pi a^2$$

For a tip radius of 75 nm, a total applied force of 16 nN (1 nN applied and 15 nN of adhesive force[29], and 77 GPa for the elastic modulus, the contact area is estimated to be 20 nm^2. Assuming full coverage of sulrfur groups on the substrate in a $(\sqrt{3}\times\sqrt{3})R30°$ overlayer structure[68,69], the packing density of the molecules is approximately $4.5*10^{14}$ molecules/cm^2, or ~5 molecules/nm^2. Thus, the number of molecules present in the contact area is approximately 100.

For each junction, the voltage was swept from –1V to +1V. The slope obtained by applying a linear fit to the data from –300 mV to +300 mV was used to estimate the low-bias resistance of the junction. Each reported resistance value is the average of the approximately 15 I-V traces performed over 3 different samples, using a single tip. A sample of the individual I-V curves for a gold-S3-gold junction are shown in Figure 3.1a. The measured electrical resistances of aromatic monothiol and dithiol molecular junctions of various lengths are shown in Figure 3.1b. Due to a consistent tip radius across the measurements the number of molecules in all junctions is estimated to be approximately the same, which allows a direct comparison of the junction resistance.

These measurements show that the electrical resistance of the monothiol junctions is at least an order of magnitude larger than the corresponding dithiol junctions. A similar trend has been observed in previous studies on aliphatic and aromatic molecular junctions[26,70].

The value of the tunneling decay parameter, β, for both monothiol and dithiol junctions is calculated to be approximately 0.14 Å, which is comparable to previous measurements with similar aromatic molecules.

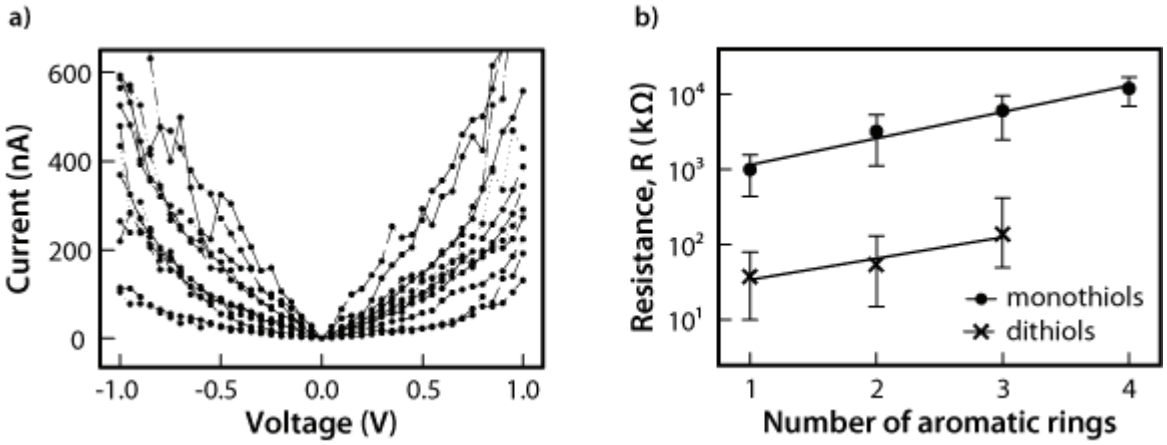

Figure 3.1 – Current-voltage characteristics for various aromatic thiol junctions. a) individual curves for one gold-S3-gold junction. Currents are plotted as absolute values. b) average low-bias resistances for monothiol and dithiols junctions of various lengths.

TRANSITION VOLTAGE SPECTROSCOPY OF MONOTHIOLS

TVS is a well-established analysis technique that enables a direct estimation of the position of the closest molecular orbital with respect to the Fermi level of the electrodes. As outlined in Chapter 1, in TVS, the current-voltage characteristic of a MMMJ is analyzed by plotting a Fowler-Nordheim (F-N) curve, $\ln(I/V^2)$ against $(1/V)$. Such a plot

shows a clear minimum, called the transition voltage (V_{trans}), which is interpreted as an approximate indicator of the energetic separation ($\Delta = eV_{trans}$) between the closest molecular orbital and the Fermi level[35,38,59]. It must be noted that the TVS measurements are not performed under large bias conditions, where charging effects in the molecule would need to be taken into consideration. Therefore, the estimated energetic separation is an approximation of the zero-bias energetic separation.

To perform TVS on monothiol MMMJs, the current-voltage characteristics (Figure 3.2 inset) of the MMMJs are first obtained by sweeping an applied bias across each MMMJ while monitoring the electric current flowing through the junction. The sweep is symmetric about 0 V, and ranged from an amplitude of 2 to 3 V (i.e. the sweep ranged from between –1.0 V to +1.0V to between –1.5 V to 1.5 V). The F-N plot obtained from the I-V curve for a sample junction, Au-S3-Au, is shown in Figure 3.2. The data on this plot is an average of 10 I-V sweeps (positive side only), and shows a clear minimum. For each molecule, 10-15 junctions were examined, yielding an F-N plot for each junction similar to that found in Figure 3.2. To obtain V_{trans}, the minima of the F-N plots for a particular molecular junction were averaged. The results are shown in Figure 3.3. For example, for Au-S3-Au, the positive half of the plots yield an average minimum at ~0.69 ± 0.08 V. The error represents the standard deviation of the minima. This value, and those of other junctions with different molecular lengths, is in excellent agreement with TVS measurements of Au-S3-Au junctions reported in an earlier study that also utilized conductive AFM and crossed wire methods[59].

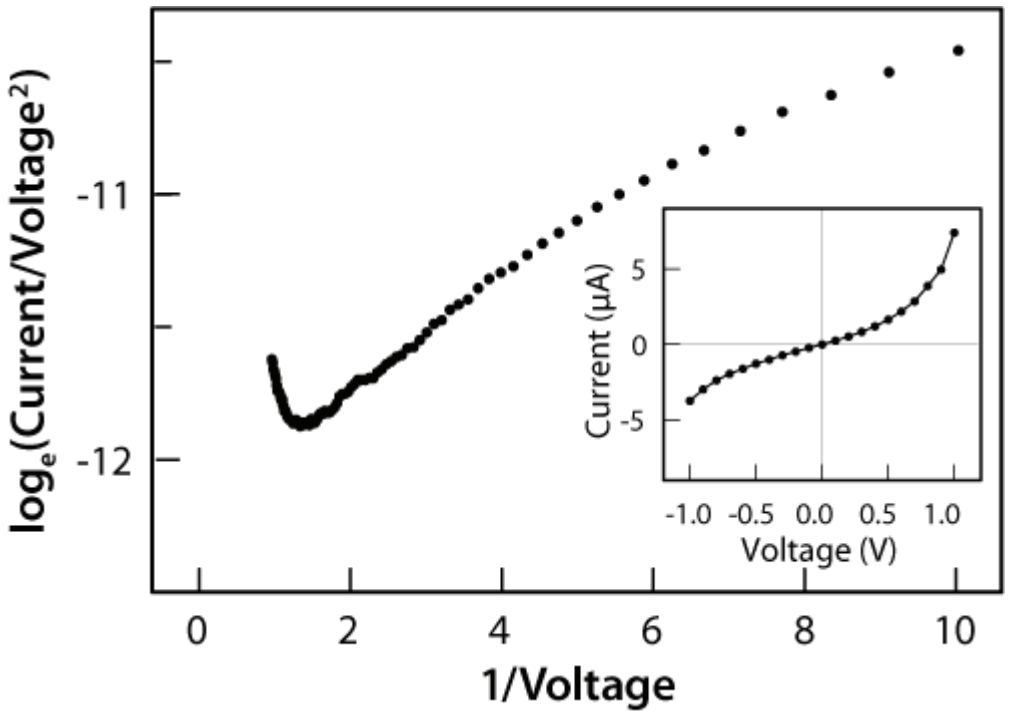

Figure 3.2 – Positive portion of the averaged Fowler-Nordheim plot for gold-S3-gold junctions. The minimum suggests that the position of the closest molecular orbital is approximately 0.69 eV away from the Fermi energy. The inset shows the averaged I-V curves of the gold-S3-gold junctions, which was used to generate the F-N plot. The curve is an average of a total of one hundred measurements, performed over ten different junctions, where ten I-V measurements were obtained for each junction.

As noted in Chapter 1, while the F-N plots in TVS were originally interpreted by modeling the molecule as a tunneling barrier, recent studies[38,41] have shown that TVS is consistent with the Landauer model of transport adopted here and allows for an estimation of the position of the closest molecular orbital. This suggests that the zero-bias energetic separation of the closest molecular orbital to the chemical potential is approximately 0.69 eV.

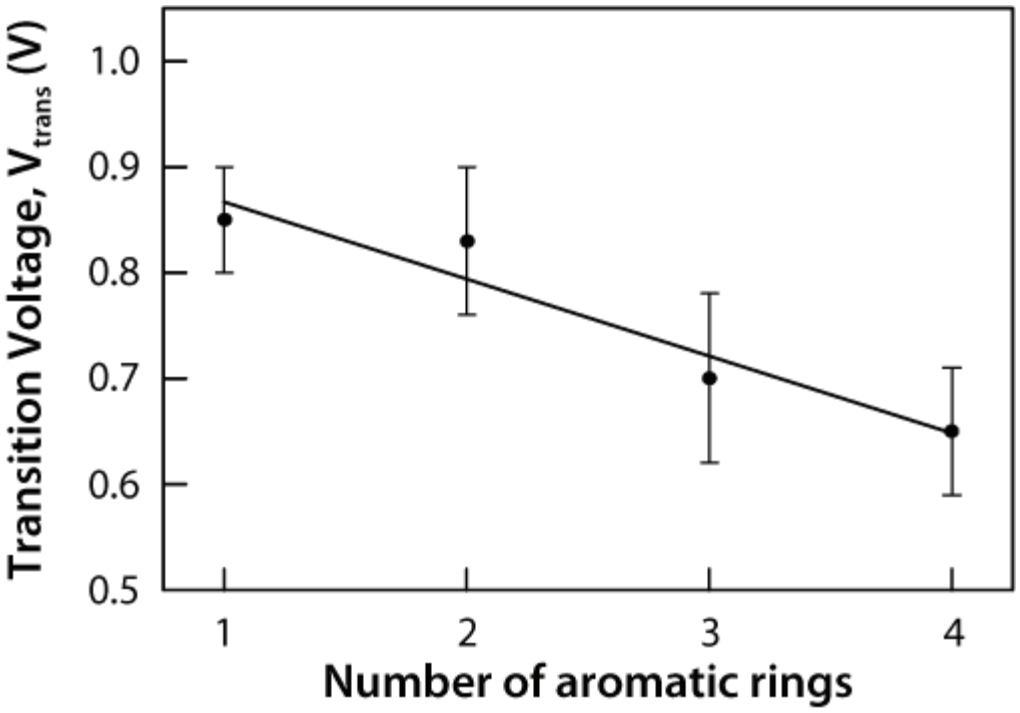

Figure 3.3 – Transition voltage of aromatic monothiol molecular junctions as a function of length (number of rings). Each point is the average of the minima obtained on the F-N plots for 10-15 junctions, and the error is the standard deviation of these minima.

Figure 3.3 presents the transition voltage of a series of aromatic thiol molecules as a function of length (one to four phenyl rings). This suggests that the separation between the Fermi level and the closest molecular orbital decreases with increasing length. This has been observed for the same or a similar series of molecules both computationally[41] as well as by AFM[35,59] and STM[70] based experiments. This is in contrast to studies done on alkanethiols, showing no length dependence of the transition voltage[59].

While the F-N plot can be drawn for either positive or negative voltages, the positive half of the I-V response is conventionally chosen[59]. This corresponds to a scenario where the substrate is grounded and a positive voltage is applied to the cantilever tip. We also plotted the negative side of the voltage sweeps on an F-N plot; comparison of the positive and negative sides of the sweep for a Au-S3-Au junction are shown in Figure 3.5. The

negative voltage values yield no minimum. Shown in Figure 3.4 is an asymmetric junction as described by the Landauer model, assuming HOMO-dominated transport. The thiolated side is strongly coupled by a chemical bond to the substrate electrode. Because the coupling is asymmetric, the energy of the molecular orbitals will be asymmetrically affected by the chemical potential of the two electrodes. Whereas the orbital level of a symmetric junction would remain at the zero-bias position relative to the electrodes, the orbital level of an asymmetric junction would follow the potential of the electrode to which it is more strongly coupled. When a negative potential is applied to the tip (the weakly-coupled electrode) the chemical potential of the tip shifts toward the LUMO of the molecule. The estimated HOMO-LUMO distance for conjugated molecules is 4 eV[15]. Since the distance between the LUMO and the chemical potential, it is reasonable that no transition voltage is observed within the range of our applied voltage.

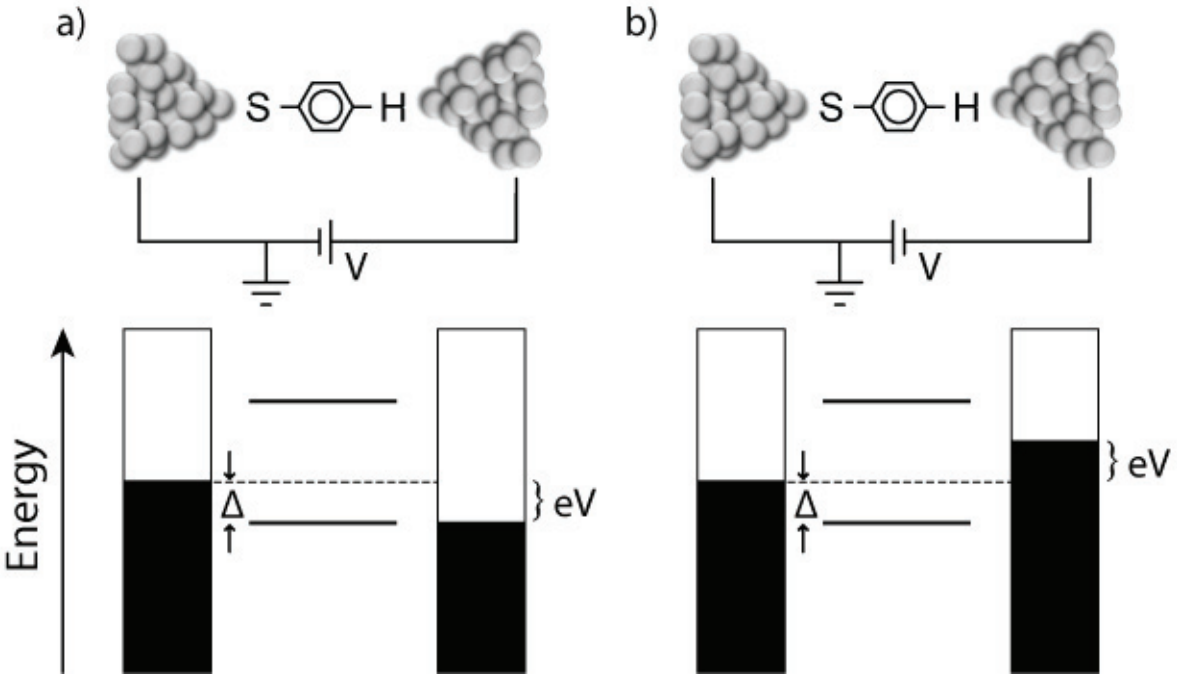

Figure 3.4 – Schematic of the effect of asymmetry on the effect of bias polarity on the electronic structure of a benzenethiol junction. HOMO-dominated transport is assumed here. a) a positive voltage is applied to the weakly coupled side of the molecule. b) a negative potential is applied to the weakly coupled side of the molecule.

Analysis and comparison of both the positive and negative sides of experimentally obtained F-N plots have not been performed with any great detail. Most papers present the F-N graph for the positive half of a voltage sweep, and do not mention the results of the negative side[59,71]. However, computational work has predicted that the F-N graphs for symmetric versus asymmetric molecules should be different. Our current study reports TVS results for a monothiol series, which comprises asymmetric molecules. As will be discussed in Chapter 5, performing TVS on symmetric molecules can yield insight on the validity of computational models, as well as determining whether the difference in the coupling geometry of the molecules to the tip and substrate plays a significant role in the electrical properties of the junction.

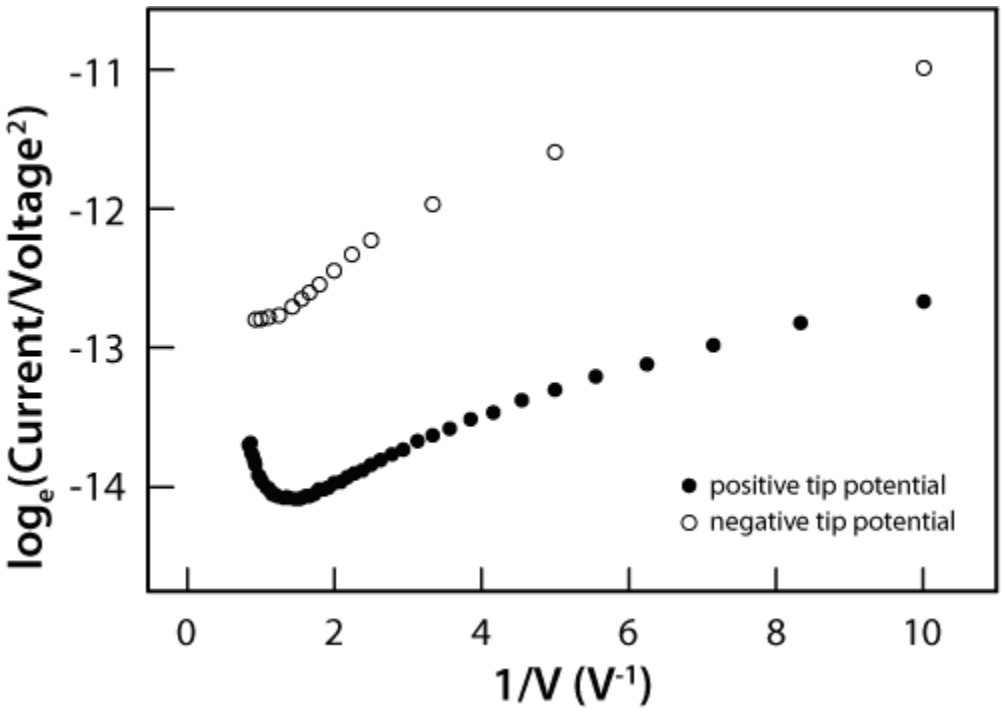

Figure 3.5 – Fowler-Nordheim plots of both positive and negative portions of a voltage sweep for a gold-S3-gold junction. A minimum was only observed for the positive portion of the sweep.

TRANSITION VOLTAGE SPECTROSCOPY IS AN INTRINSIC PROPERTY

Assuming that there are no intermolecular interactions in the monolayer[15] and that the molecules are contacted equally well by the tip such that all junctions are identical, the molecules can be considered as resistors in parallel. The total resistance of all the junctions can then be related to the number of molecular junctions, *N*, formed between the tip, the monolayer, and the substrate[26]:

$$R = G^{-1} = \left(\sum_i G_{junction}\right)^{-1} = \left(NG_{junction}\right)^{-1} = \left(N\frac{2e^2}{h}T(\varepsilon)\right)^{-1} = \frac{h}{2e^2NT(\varepsilon)}$$

The more junctions that are present, the lower the resistance should be. One would also expect that the resistance (number of junctions) is related proportionally to the contact area or tip radius. A number of preliminary studies have been performed[15,29] which reasonably suggest that a correlation exists between the tip radius/contact area and junction resistance of a molecular junction.

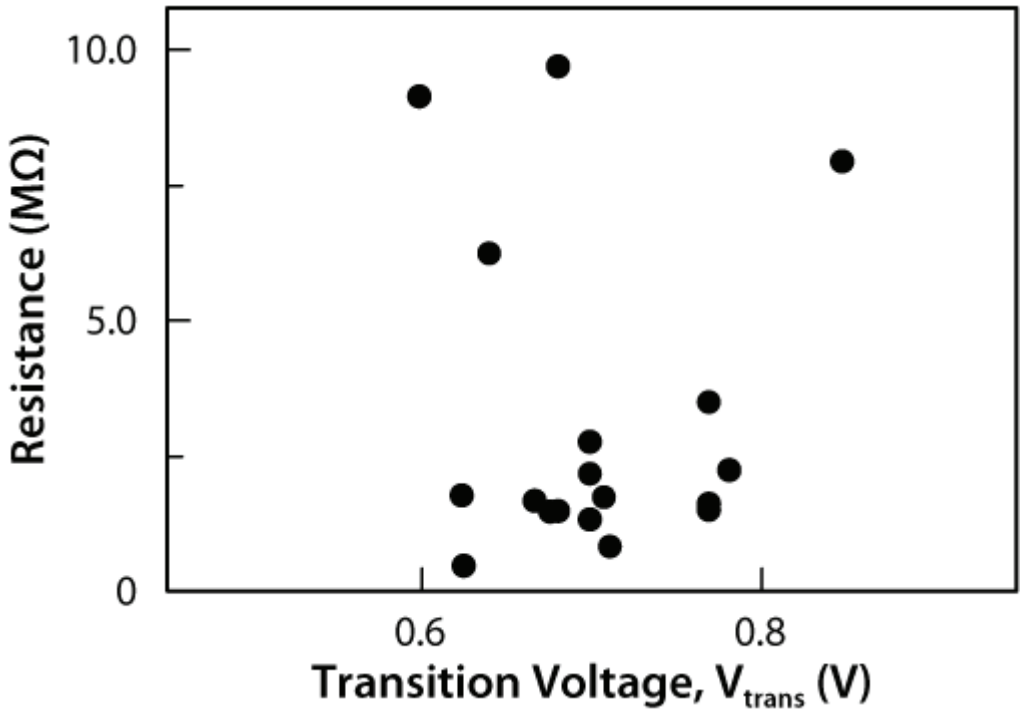

Figure 3.6 – Plot of resistance versus transition voltage for several gold-Au-gold junctions. There is no discernable trend, indicating that the transition voltage is an intrinsic property that is independent of the number of junctions formed.

The low-bias resistance of each junction was plotted against the junction's transition voltage, as shown in Figure 3.6. There is no observed correlation between that junction resistance and the transition voltage, suggesting that any intermolecular interactions do not play a role in altering the electronic properties of a single junction, and also that the transition voltage is an intrinsic property of the junction that is independent of the number of junctions present.

QUESTIONS ARISEN ABOUT ELECTRONIC STRUCTURE

To summarize the findings presented in this chapter, TVS analysis of MMMJs can provide us an estimate of the energetic separation of the Fermi level and the molecular

level through which conduction primarily occurs, However, TVS cannot conclusively identify the relative alignment of the orbitals – that is, TVS cannot be used to determine whether transport occurs through the HOMO or the LUMO. In order to discover this information, we measure the thermoelectric characteristics of the junctions. Performing a measurement of the thermopower of the junction can unambiguously reveal which molecular orbital is closer to Fermi level. As will be subsequently discussed in this work, a positive thermopower is associated with a HOMO that is closer to the chemical potential, indicating hole dominated (p-type) transport. In the other scenario, transport is LUMO dominated (n-type) and is related to a negative thermopower. Figure 3.7 illustrates the two scenarios that thermoelectric measurements can be used to distinguish.

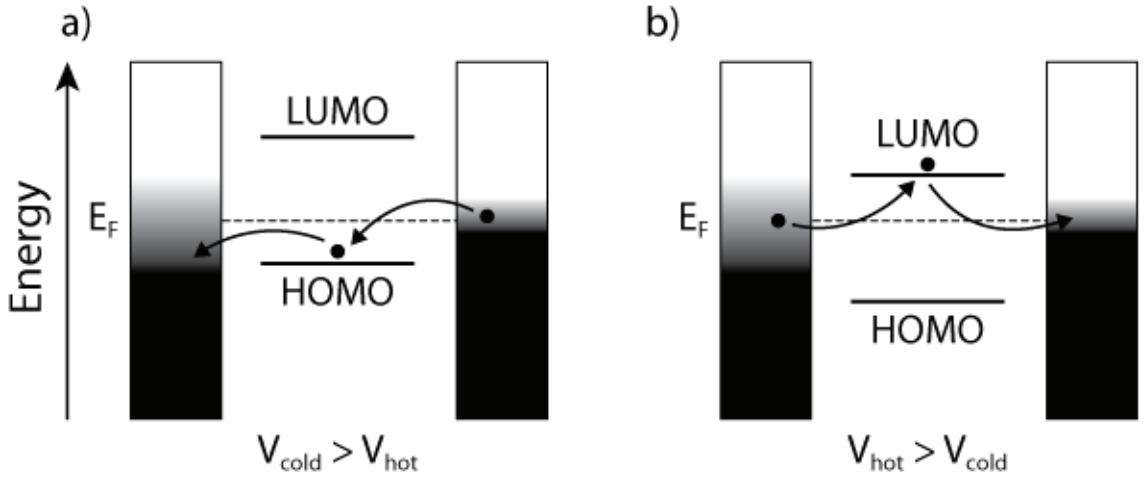

Figure 3.7 – The two scenarios that a Seebeck coefficient measurement can distinguish: having the HOMO orbital closer to the Fermi level corresponds to a positive Seebeck coefficient, whereas the other scenario results in a negative Seebeck coefficient.

Chapter 4

Thermoelectric Properties of Molecular Junctions

Obtaining the Junction Thermopower from Thermoelectric Voltage Measurements

Thermoelectric voltage measurements were performed by applying a temperature different across the monolayer and measuring the resulting open-circuit voltage between the tip and substrate. The substrate was grounded while a bias voltage was applied to the AFM tip (Figure 2.7). Temperature differentials ranging from 0 K to 12 K were applied in steps of 3 K and a home-built voltage amplifier circuit based on Poler's design[72], was used to measure the resulting thermoelectric voltages. An electronic relay circuit was built to allow fast switching between the current and voltage amplifier for concurrent electrical and thermopower measurements. Due to the geometry of the experimental apparatus, the measured open-circuit voltage is actually the sum of the potential of the junction and the potential developed across a gold wire that connects the substrate electrode to one of the amplifier leads. Below is a derivation of the relationship between measured voltage and the junction Seebeck coefficient.

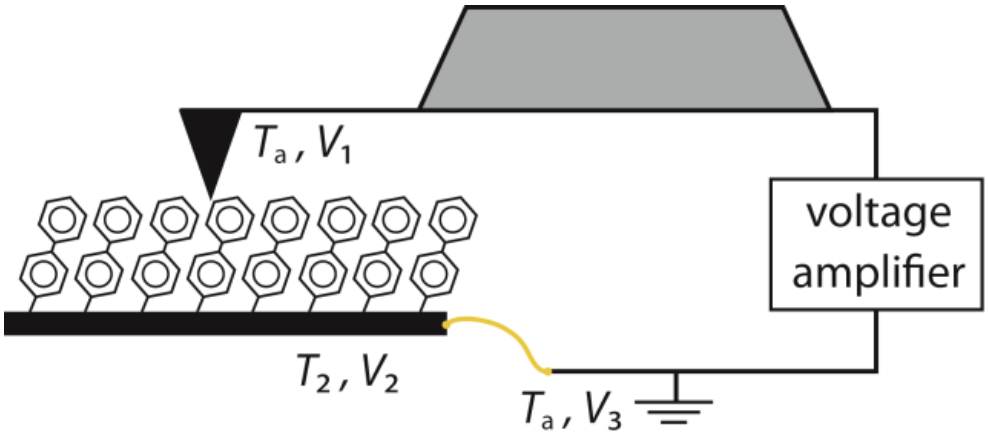

Figure 4.1 – Schematic diagram of voltages and temperatures across the metal-molecule-metal junctions formed in this work. A short gold wire connects the substrate to the triaxial copper wire that leads to the voltage amplifier.

Thermopower is defined by the following relation:

$$\vec{E} = S\nabla T \Rightarrow -\nabla \mathrm{V} = \mathrm{S}\nabla \mathrm{T}$$

where $\vec{E}$ is the electric field. On integrating,

$$V_2 - V_1 = -S_{junction}(T_2 - T_a)$$

where V_2 is the voltage at the junction of the molecule and the substrate and V_1 is the voltage at the tip (Figure 4.1). T_2 is the temperature of the heated substrate and T_a is the ambient temperature. In addition to the temperature drop across the junction, there is also a temperature drop across the gold wire connecting the substrate to ground:

$$V_3 - V_2 = -S_{Au}(T_a - T_2)$$

where V_3 is ground (the end of gold wire). Upon adding the above two equations,

$$V_3 - V_1 = \left(S_{Au} - S_{junction}\right)(T_2 - T_a)$$

It is then clear that the junction Seebeck coefficient, S_{junction}, is given by:

$$S_{junction} = S_{Au} - \frac{V_3 - V_1}{\Delta T}$$

CONTROL EXPERIMENTS ON THERMOPOWER

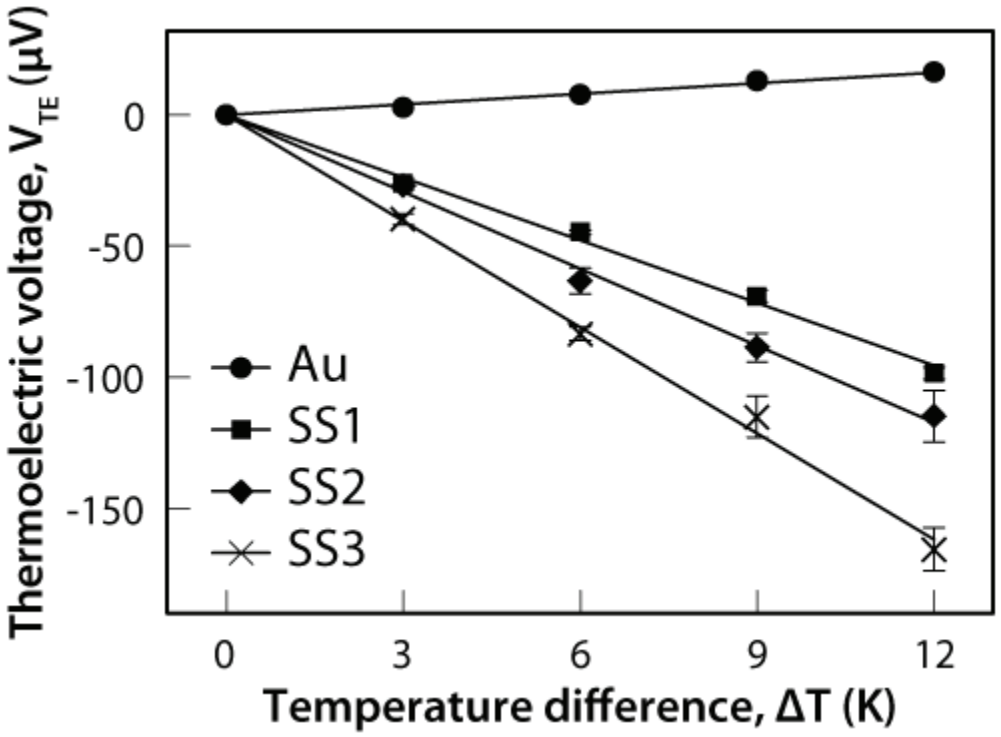

Figure 4.2 – Measured thermoelectric voltages for gold-aromatic dithiol-gold junctions as well as those for a gold-gold point contact.

Thermopower measurements were performed on freshly cleaved gold surfaces coated with no organic monolayer to ensure that the thermoelectric voltages observed were indeed arising from the presence of molecules. It has been shown that the thermopower of a Au-Au point contact junction is dependent on the contact resistance[73]. The thermopower can vary between 0.1 μV/K for small contact resistances (mΩ), up to 1.3 μV/K for larger contact resistances of around 100 Ω. Figure 4.2 shows a representative control experiment where the thermopower of a Au-Au junction with a resistance of ~98 Ω is measured. These measured thermoelectric voltages are much smaller than the voltages measured using molecule-coated Au surfaces, clearly showing that the molecules are the source of the observed voltages in our experiments.

EFFECT OF LENGTH ON THERMOPOWER

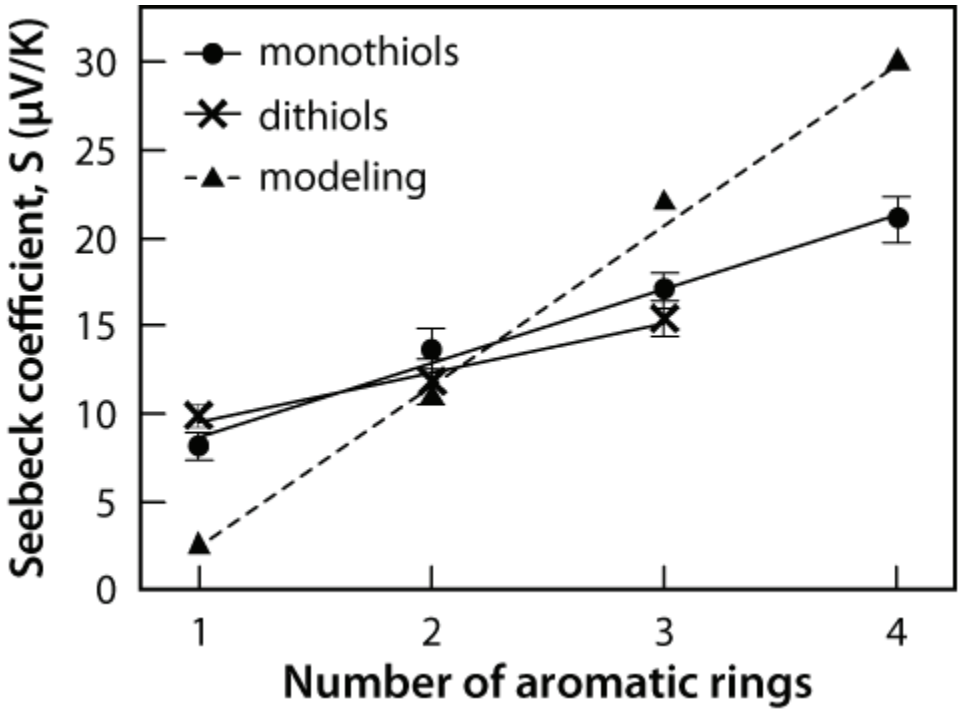

Figure 4.3 – Plot of Seebeck coefficients for metal-molecule-metal junctions formed from monothiol and dithiol monolayers of varying molecular length, along with the computed values for the Seebeck coefficient of dithiol junctions.

The thermoelectric voltages ΔV are measured by a custom-built voltage amplifier by trapping dithiol molecules between a gold-coated AFM tip and a heated gold substrate are shown in Figure 4.2. The displayed thermoelectric voltages represent the mean of the measured voltage in ten independent measurements; where the error bars represent the standard deviation. The magnitude of the measured thermoelectric voltage increases linearly when the temperature differential (ΔT) applied across the molecular junction is increased. Using this expression derived above for $S_{junciton}$ and the measured thermoelectric voltages (Figure 4.2), the Seebeck coefficient corresponding to junctions based on SS1, SS2, SS3 molecules is found to be (+9.8 ± 0.6) μV/K, (+11.7 ± 1.3) μV/K, and (+15.4 ± 1.0) μV/K respectively.

An increasing trend in the junction Seebeck coefficient for increasing molecular length can be predicted when transport through the molecules is modeled by a tunneling barrier. As noted in Chapter 1, the transmission function can be expressed as

$$T(E) \propto \exp\left(-\frac{\sqrt{2mE}}{\hbar}L\right); \quad \ln[T(E)] \propto -\frac{\sqrt{2m\alpha E}}{\hbar}L$$

Substituting this into the equation for the Seebeck coefficient obtained using the Landauer equation,

$$S_{junction} \propto -\frac{\pi^2 k_B^2 T_1}{3e}\frac{\partial}{\partial E}\left(-\frac{\sqrt{2mE}}{\hbar}L\right)\Big|_{E=\mu_1} = \frac{\pi^2 k_B^2 T_1}{3e\hbar}\sqrt{\frac{2m}{E_b}}L$$

Here, E_b is the tunneling barrier height. Though $S_{junction}$ is dependent on both the barrier height and the molecular length, the linear length dependence of $S_{junction}$ dominates over its dependence on barrier height (inverse square root). In addition, transition voltage spectroscopy suggests that E_b diminishes as the length of the molecule increases. According to the above equation, a decreasing barrier height will cause an increase in the value $S_{junction}$. It is also important to note that this change in E_b is relatively small compared to the change in length (e.g. from 0.85 *eV* to 0.65 *eV* for molecules with one and four benzene rings, respectively – or about 25% change in E_b compared to the 400% change in length). Thus, the dominating factor affecting $S_{junction}$ is the molecular length. This is observed in the approximately linear relationships obtained in our experiments, as depicted in Figure 4.3.

Effect of Contact Coupling Strength on Thermopower

Past theoretical studies[24] have elucidated the effect of contact coupling strength on the thermoelectric properties of junctions. These computational studies suggest that when

coupling of a molecular junction with one of the electrodes is weakened, the Seebeck coefficient will remain relatively invariant even though the electrical conductance of the junction decreases significantly. In order to test this hypothesis, we experimentally studied the thermoelectric characteristics of junctions fabricated from self-assembled monolayers of monothiol and dithiol molecules (Figure 2.8). The electrical resistance of these junctions was reported in Chapter 3. The measured Seebeck coefficients of the monothiol and dithiol junctions are listed in Table 4.1. Remarkably, the change in coupling strength results in only a marginal effect on the Seebeck coefficient—the difference in the thermopower of monothiol and dithiol junctions is only a few percent and is in strong contrast with the large difference (an order of magnitude) in the electrical resistance of molecular junctions.

No. of rings	Experimentally measured values (μV/K)			Computed dithiol values (μV/K)
	Monothiols	Dithiols	Previous single molecule dithiol studies[74]	
1	8.1 ± 0.8	9.8 ± 0.6	8.7 ± 2.1	2.4
2	13.6 ± 1.2	11.7 ± 1.3	12.9 ± 2.2	10.8
3	17.0 ± 1.0	15.4 ± 1.0	14.2 ± 3.2	21.9
4	21.0 ± 1.3	–	–	29.9

Table 4.1 – Experimentally measured Seebeck coefficients of monothiol and dithiol junctions are presented along with the computed Seebeck coefficients of the same dithiol junctions. The Seebeck coefficients of single-molecule dithiol junctions obtained in an earlier work are also presented for comparison.

This behavior is well explained using a simple model by Paulsson and Datta[24]. In this picture the transmission function of a weakly bound junction is related to the transmission of a strongly bound junction by a scaling factor ($0 < c < 1$):

$$T(E)_{weak} = c \times T(E)_{strong}$$

In our case, the monothiol and the dithiol junctions represent the weakly and strongly bound junctions, respectively. Considering the equations for conductance and for thermopower derived using the Landauer equation, it is evident that decreased contact coupling lowers the electrical conductance, whereas the Seebeck coefficient remains invariant to changes in the coupling. Our experimental data provides the first convincing evidence that this simple theoretical model[24] can qualitatively capture the effect of weakening the coupling with one of the contacts.

INSIGHT ABOUT ELECTRONIC STRUCTURE

The sign of the thermopower of a molecular junction reveals which molecular orbital lies closer to the Fermi level. As a first analysis, we can relate the sign reversal to the electronic structure of the junction by inspecting the equation for thermopower derived from the Landauer model. This equation, derived in Chapter 1, relates the thermopower of a junction to the slope of the molecule's transmission function at the Fermi level:

$$S = -\frac{\pi^2 k_B^2 T_1}{3e} \frac{\partial \ln T(E)}{\partial E}\bigg|_{E=\mu_1}$$

If the thermopower is positive, the equation dictates that the slope of the transmission function at the Fermi level must be negative. This is true if the Fermi level is closer to the HOMO, as seen in the simple calculations using the Landauer model for a gold-benzenedithiol-gold junction[24,74]. The positive Seebeck coefficients observed in junctions formed by thiol-terminated molecules suggests that transport through these systems is p-type (HOMO-dominated). Conversely, a negative Seebeck coefficient indicates a positive slope of the transmission at the Fermi level, and would correspond to transport through the LUMO (n-type).

EFFECT OF CONTACT CHEMISTRY ON THERMOPOWER

Recent computational[75-79] and experimental work [70,76,80] suggests that end group chemistry provides an attractive route for tuning the electronic energy levels of the junction relative to the chemical potential. Here, we explore the prospect of changing the sign of the Seebeck coefficient by end group chemistry. The positive Seebeck coefficients realized with thiol terminated junctions suggest p-type transport, which is associated with the HOMO being the closest level to the Fermi energy. In contrast, a negative sign of the Seebeck coefficient would be expected to correspond to the opposite case of LUMO dominated transport. In fact, it has been hypothesized that n-type transport can be realized with isocyanide end groups[26]. In order to test this hypothesis, we designed experiments where monolayers were created from an isocyanide (–NC) terminated aromatic molecule (NC3, Figure 2.8).

The thermoelectric voltages measured for isocyanide terminated junctions are shown in Figure 4.4. The measured thermoelectric voltages indicate a negative Seebeck coefficient of (–1.0 ± 0.4) μV/K. The sign of the Seebeck coefficient confirms that transport in the isocyanides is n-type. This result is particularly insightful because previous electrical transport studies[70] of isocyanides were unable to determine whether the HOMO or the LUMO orbital is closer to E_F.

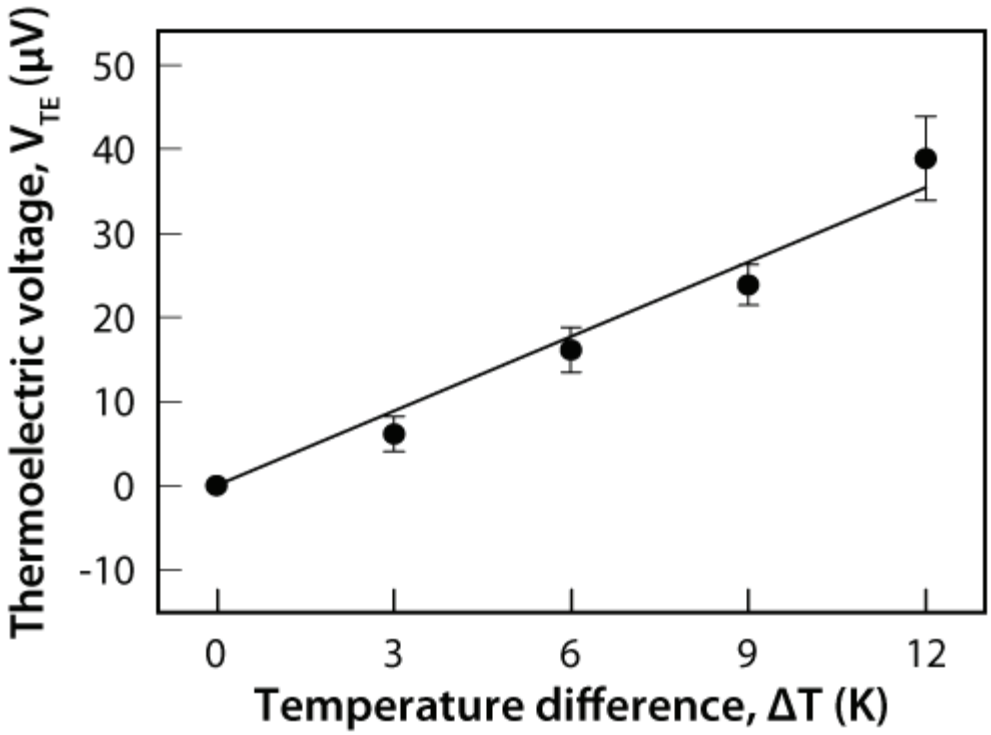

Figure 4.4 – Measured thermoelectric voltages of gold-NC3-gold junctions.

The negative Seebeck coefficient of the isocyanide junction is in contrast to the positive coefficient of the corresponding thiol terminated junction. We note that the effect of end group on the sign of the thermopower was also observed in a previous experimental study on junctions formed from monolayers of cyanide (–CN) terminated molecules[80]. The current study of isocyanide (–NC) terminated junctions not only explores the applicability of another end group to tuning thermoelectric properties but—more importantly—probes the relationship between electronic structure and the sign of thermoelectric properties.

To further verify our claim that the sign of the thermopower yields information about whether transport is HOMO or LUMO dominated, our collaborators computationally modeled the transport properties of a three ringed diisocyanide junction to analyze the sign dependence of the thermopower on the contact (Figure 4.5). For modeling

simplicity, the Seebeck coefficient of the mono functionalized molecular junction was compared to a model that involves two end groups $(NC)_2$3. This modeling scheme is justified by the previous observation that the Seebeck coefficient is invariant with coupling strength for thiol-terminated molecular junctions. The computed transmission function shows that the diisocyanide transport is dominated by the LUMO channel resulting in n-type transport. The Seebeck coefficient calculated for the 3 ring isocyanide junction (–1.6 μV/K) matches in sign with the experiments, and has a magnitude comparable to the experimentally measured value of (–1.0 ± 0.4) μV/K.

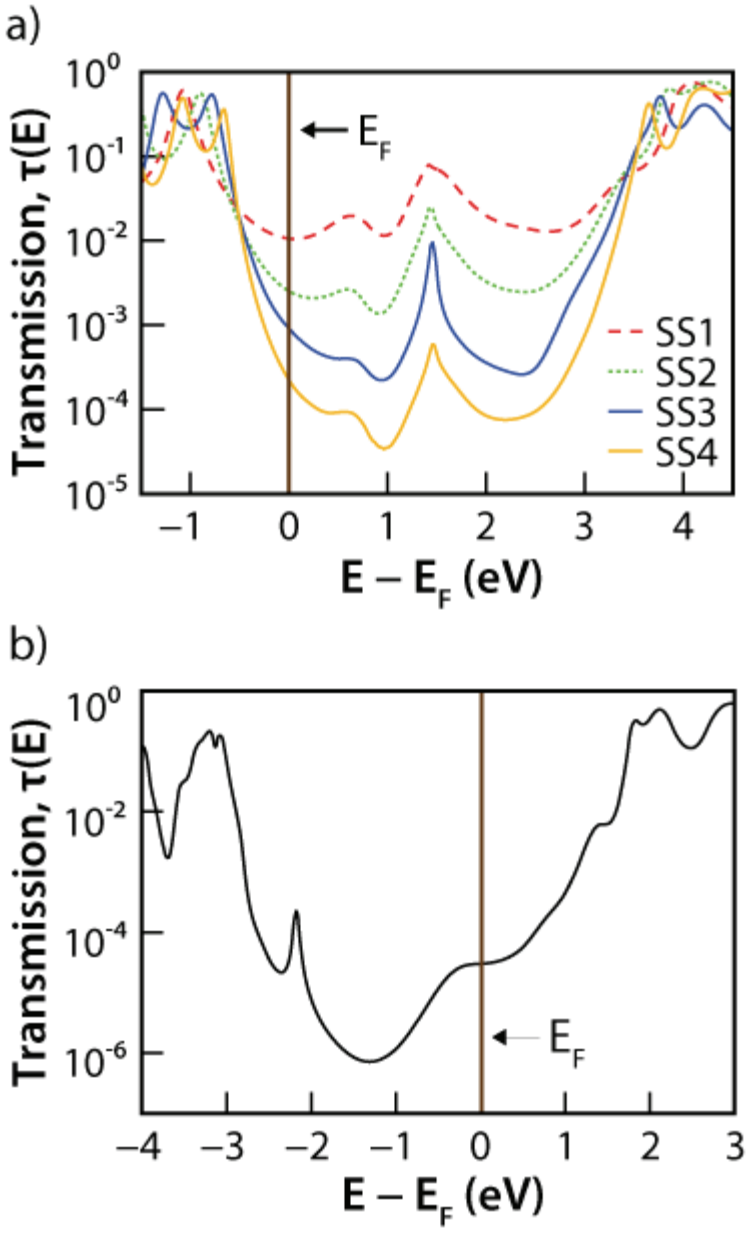

Figure 4.5 – Computed transmission functions for a) Au-aromatic dithiol-Au junctions and b) a three-ring Au-aromatic diisocyanide-Au junction.

The negative Seebeck coefficient of the isocyanide junction is in contrast to the positive coefficient of the corresponding thiol terminated junction. We relate the sign reversal to the electronic structure of the junction by observing the electronic density of states (DOS). The electronic DOS in the molecular region for SS3 and $(NC)_2$3 junctions are

plotted in Figure 4.6. The DOS for the SS3 junction shows that the transport is dominated by orbitals below the chemical potential (p-type), resulting in a positive thermopower. In contrast, the electronic DOS of $(NC)_2$3 junctions shows that transport is dominated by orbitals above the chemical potential (n-type), resulting in a negative thermopower.

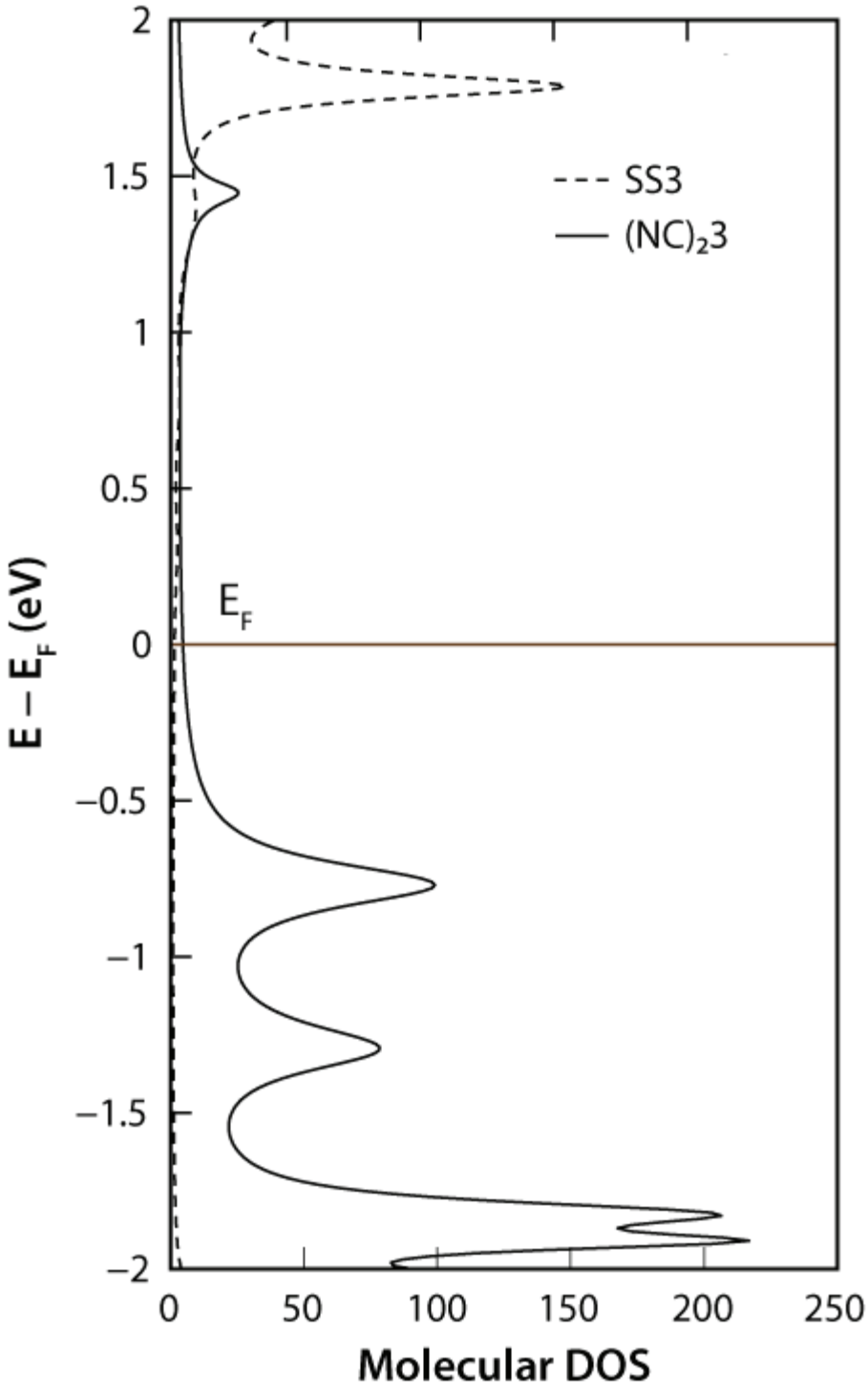

Figure 4.6 – Molecular electronic density of states around the chemical potential in the SS3 and $(NC)_2$3 junctions.

THERMOPOWER IS AN INTRINSIC PROPERTY

An important point to note about the findings in the previous two chapters is that unlike conductance measurements, both the measured thermopower and the transition voltage obtained are independent of the number of the molecules trapped in the MMMJ. The intrinsic nature of a junction's thermopower can be demonstrated analytically by using the Landauer equation for the thermopower of a MMMJ. Assuming that there are N identical, non-interacting junctions connected between two electrodes, the transmission function of the total contact area is $NT(\varepsilon)$. The total thermopower of all the junctions is then

$$S = -\frac{\pi^2 k_B^2 T_1}{3e}\frac{\partial \ln \mathrm{N}T(E)}{\partial E}\bigg|_{E=\mu_1} = -\frac{\pi^2 k_B^2 T_1}{3e}\frac{\partial \ln T(E)}{\partial E}\bigg|_{E=\mu_1}$$

Therefore, the technique described here is not affected by variations in the radii of AFM tips (which leads to a variation in the number of molecules trapped), thus making it possible to obtain repeatable results. It was because of this that our tips could be reused and recoated with gold multiple times when performing thermoelectric measurements. Only when absolute I-V values were needed were exclusively fresh tips used, and only once per sample. This finding of the independence of thermopower and the transition voltage on the number of molecules contacted offers support towards the conclusion that intermolecular interactions among species forming the monolayer are insignificant in conduction compared to the through-molecule dependence[15].

UNCERTAINTY IN THERMOPOWER MEASUREMENTS

Each thermoelectric voltage plotted in Figure 4.2 and Figure 4.4 was the average of 10 independent measurements, where the error bars represent the standard deviation. We believe that the uncertainty in our thermopower measurements arises primarily from two sources: first, the microscopic details of metal-molecule contacts across the junctions measured are different. In fact, this has been discussed in detail in the past by Malen *et al*.[81,82] We believe that the origin of the increased uncertainty with the temperature differential applied lies in the increased drift of the AFM tip with temperature[83]. In fact, we observe that as the temperature differentials are increased to ~30 K (much higher temperature differentials than those reported here) the current AFM system becomes unstable, making it impossible to obtain reliable measurements. However, we believe that this is not an intrinsic limitation of the technique but only reflects the limitations of our current commercial AFM hardware. Secondly, there is a 5% uncertainty in the applied temperature differential, which is also accounted for in the reported standard deviation for the Seebeck coefficients.

Chapter 5

Conclusions and Future Work

We have shown that our new AFM-based technique can answer important questions regarding the electronic structure of molecular junctions: namely, the identity of the molecular orbital closest to the Fermi level and the magnitude of this energetic separation. In addition, we have also used this technique to perform preliminary studies of the dependence of molecular structure, chemical composition of electrodes, and end groups on the thermoelectric properties of molecular junctions. Based on an analysis of our thermopower measurements using the Landauer model, electronic transport through aromatic thiols of various chain lengths is HOMO dominated. Furthermore, the linearly increasing value of thermopower for increasing molecular length suggests that the HOMO level moves closer to the Fermi level for longer molecules. This reduction in energetic separation between the closest molecular orbital and the Fermi level was also suggested by the increasing transition voltage with increasing length for the same series of aromatic thiol molecules as interpreted using the Landauer model. Comparison of thermopower trends of a monothiol series with a dithiol series confirms that coupling strength does not play a role in the magnitude of a junction's thermopower, or equivalently, the relative electronic alignment of molecular orbitals with respect to the Fermi level of the electrodes is identical for monothiols and dithiols. However, the

change in sign of the thermopower of a junction formed from isocyanide-terminated molecules suggests a change from HOMO- to LUMO-mediated transport. This indicates that contact chemistry plays a large role in determining the electronic structure of the junction.

FUTURE WORK

Several groups have recently presented computational studies on the effect of molecular symmetry on the value of the transition voltage[23,39,41]. According to their studies, asymmetry of the molecule can affect the ratio of the frontier orbital separation and the transition voltage (i.e. $(E_{orbital} - E_F)/V_{trans}$) by a factor of 2. This can be seen by using the Landauer picture for simple one-level transport and accounting for the fact that the potential of the molecular levels can shift with respect to the electrodes (see Figure 5.1). Symmetry also affects the shape of the positive and negative sides of the Fowler-Nordheim plot when compared with each other.

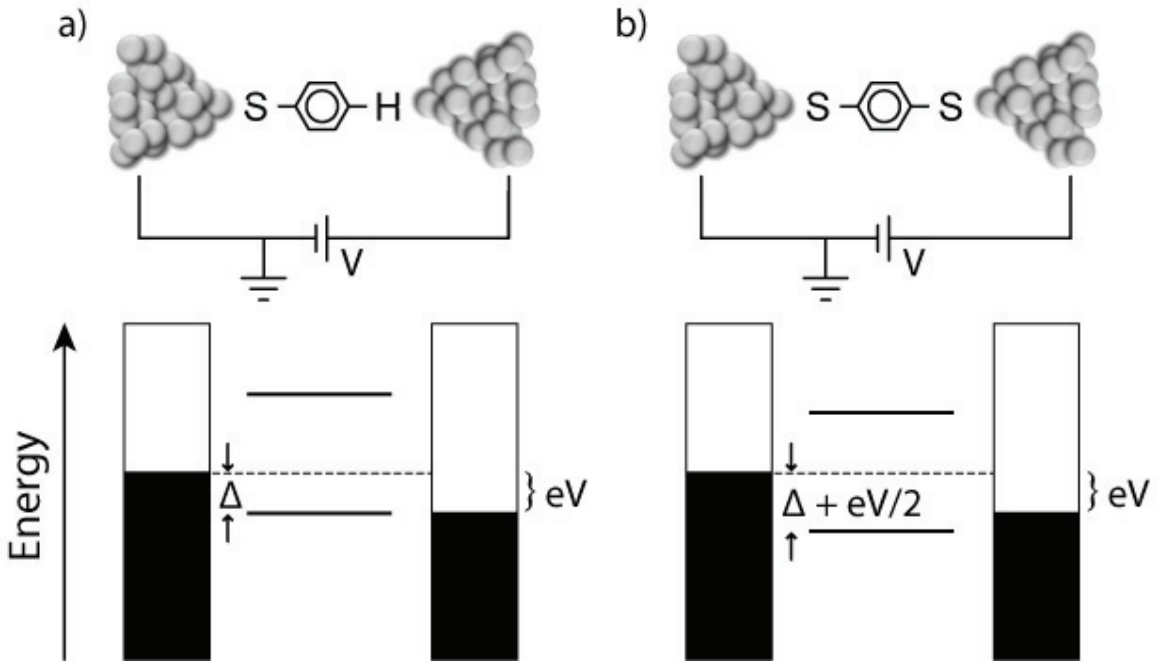

Figure 5.1 – The effect of symmetry on the alignment of molecular orbitals with respect to the electrode Fermi levels for a given applied bias V. Only the frontier orbitals (HOMO and LUMO) are shown for clarity. a) a benzenethiol junction. The molecule is strongly bound to the electrode that the thiol is bound to. Therefore, the molecular orbitals will remain aligned to the Fermi level of this strongly-bound electrode. b) a benzenedithiol junction. The molecular orbital is strongly coupled to both electrodes, and will shift by eV/2.

No high-bias measurements of aromatic dithiols using an AFM platform have yet been reported, even though several studies on dithiols have been performed on STM apparatuses. This could be due to the higher current densities present in such conjugated junctions or the increased electrostatic/capacitive effects at higher applied biases that pull the tip towards the substrate, causing a short circuit. The strong coupling of the thiol group on the molecule results in strong interactions with both the substrate and the AFM tip. This would cause even nanometer-sized drifts to be a potential cause for concern, as severed thiol bonds can tear off the gold layer on the tip, rendering it non-conductive. Furthermore, comparison of the positive and negative sweeps of TVS has not been experimentally studied with any great detail. Only one paper cites any reference to a complete analysis of both sides of the voltage sweep for a monothiol series, and in this paper, there was no observable minimum for negative voltages[35]. Most papers present the F-N graph for the positive half of a voltage sweep, and do not mention the results of the negative side.

Performing full-sweep TVS measurements on dithiol junctions using an AFM based approach would yield experimental verification of the effect of symmetry on the analysis technique. This goal can likely be achievable on a system with reduced drift and which has a force feedback system that can compensate for capacitive effects. Ultra-stable AFM

systems have recently been built[84,85] and could be promising platforms for future work with aromatic dithiol junctions.

Though this paper presents findings on thermopower in light of their revealing electronic information about molecular junctions, there is also a long-term prospect of utilizing molecules as efficient thermoelectric devices. The ability to simultaneously measure the thermopower and electrical conductance of molecular junctions not only allows the probing of the electronic structure of MMMJs but will also provide an important tool for exploring the possibility of creating high efficiency organic based thermoelectric materials. Recently, Finch *et al.* showed that the computed thermopower of molecules could be tuned by modifying the side groups[86]. For a particular molecule shown in Figure 5.2, they computed large thermopowers of up to 670 μV/K at room temperature.

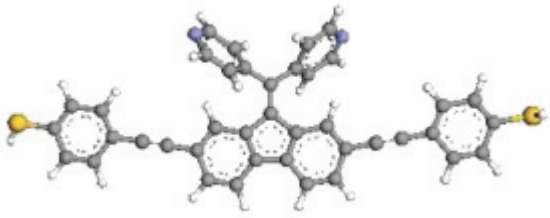

Figure 5.2 – A schematic of CSW-470-bipyridine (CSW-479), modeled by Finch et al.[86] The thermopower of a single-molecule junction formed by CSW-479 reached up to 670 μV/K for certain rotation angles of the side group, and the figure of merit reached about 100.

The thermoelectric figure of merit of a material is defined as

$$ZT = \frac{S^2 \sigma T}{k}$$

where S is the material's Seebeck coefficient, σ is the electrical conductivity, T is the average temperature, and k is the thermal conductivity. It is a measure of the efficiency of a material in converting thermal gradients to an electric potential. A greater ZT indicates

a greater thermodynamic efficiency, subject to certain provisions, particularly that the two materials in the couple have similar Z. ZT is therefore a method for comparing the potential efficiency of devices using different materials. Values of 1 are considered good; values in the 3–4 range are essential for thermoelectrics to compete with mechanical devices in efficiency. To date, the best reported ZT values are around 2[87,88].

As is apparent from the above formula, increasing the Seebeck coefficient and the electrical conductivity of the molecule, while decreasing the thermal conductivity, would increase the figure of merit of a junction. From the simple Landauer picture of a single-electron level, if the chemical potential is close to either the HOMO or the LUMO level, the thermopower can be increased due to the steeper slope of the transmission function near the orbitals. Also, the electrical conductance would also be increased due to the increased magnitude of the transmission function here. Measurements of the thermal conductance per unit area of molecular junctions show that this property is invariant with molecular length, and remains around 30 MW m^{-2} K^{-1} [89,90]. Thus, if the Fermi energy of a junction was tuned to be closer to the HOMO or LUMO level, the figure of merit of the molecule could be increased.

Frisbie *et al.* recently synthesized a series of long conjugated oligoimine[71] (ONI) molecular wires. F-N plots of the I-V response of these molecules exhibit a transition voltage of 0.3 – 0.5 V, which is almost twice as small as the transition voltages for aromatic monothiols studied in this work. These transition voltage values suggest that the distance between the HOMO and the Fermi energy is significantly smaller than that of aromatic monothiols; the conductance of the series is comparable to those of the

monothiols. New series of molecules could serve as a starting point for studies on engineering molecular structure to optimize the figure of merit of molecular junctions.

Appendix 1

Thermal Modeling of the Temperature Gradient across a Metal-Molecule-Metal Junction

In order to accurately measure the Seebeck coefficient of MMMJs, a clear understanding of the temperature distribution across the junction is necessary. Since the experiment is performed in an ambient environment, the primary channels for heat transport from substrate to thermal reservoir to which the micro-cantilever is anchored, are: 1) heat conduction between the tip and substrate through the self assembled monolayer (SAM), and 2) heat conduction between substrate and micro-cantilever through the ambient air. It has been shown[66] in past work that heat transport through the air is much larger than the heat transport through the nanoscale point contact at the tip-molecule-substrate junction. Further, a detailed mathematical model has been developed and verified to describe temperature distributions in such point contacts. A brief outline of the mathematical model and the pertinent results are provided here.

The temperature distribution of the metal-molecule-metal junction shown in Fig. 1 can be modeled using a one dimensional heat conduction equation[66]

$$\frac{d}{dy}\left[A_t(y)k_t(y)\frac{dT(y)}{dy}\right] - p(y)h_a(y)\tan(\theta)(T(y) - T_{sub}) = 0$$

Here k_t and A_t are the thermal conductivity and the cross-sectional area of the tip respectively, T is the temperature of the tip, T_{sub} is the substrate temperature, θ is the half angle of the conical tip, and p is the perimeter of the cross section of the tip. For each point on the perimeter of the tip, it is assumed that heat is conducted by air between the point and a point immediately below on the substrate. These two points are treated as if they are located on two parallel plates.

This simplified picture of heat transport in air is captured in the second term of the above equation. The distance between the two corresponding points on the tip and substrate is $(y + d)$. The air conduction coefficient h_a has different forms for different regimes of $(y + d)/l$, where l is the mean free path of molecules in air (~60 nm under ambient conditions)[91]. For $(y + d)/l > 100$, a constant temperature gradient is assumed at the air gap and $h_a = \alpha K_a/(y + d)$, where K_a is the thermal conductivity of bulk air and α is a geometry factor to accommodate the fact that the tip and the substrate are not exactly two parallel plates and is approximately 0.8 ± 0.1 for our geometry, as shown earlier. For $1 < (y + d)/l < 100$, a temperature discontinuity may develop as intermolecular collisions become less frequent and molecules arriving at the solid surfaces are unable to come into equilibrium with the surface. In this so-called slip regime,

$$h_a = \frac{(aK_a)/(y+d)}{1+2fl/(y+d)}; \qquad f = \frac{2(2-A)\gamma}{A(\gamma+1)Pr}$$

where A is a thermal accommodation coefficient (~0.9 for air), γ is the ratio of air heat capacities and Pr is the Prandt number. In a regime where $(y + d)/l < 1$, air molecules are transported ballistically from one surface to another, and h_a can be written as

$$h_a = \frac{aK_a'}{(y+d)(1+2f)}; \qquad K_a' = \frac{CV(y+d)}{3}$$

where K_a' is the thermal conductivity of air in the free molecule flow regime, and C and V are the heat capacity and root-men-quare velocity of air molecules, respectively.

The above equations can be solved numerically for the current experimental setup using the appropriate boundary conditions for the substrate temperature and the AFM cantilever body temperature where it is in connectd with the thermal reservoir. The calculations show that for a silicon cantilever (used in our experiment with length 125 μm, width 35 μm, thickness 1 μm, an with a half cone angle of 18°) even when the tip is brought into contact with the SAM, the temperature at the very end of the tip is less than $T_{ambient}$ + $0.05(T_{\text{sub}} - T_{ambient})$, where $T_{ambient}$ and T_{sub} are the temperatures of the reservoir and substrate. This means the increase in tip temperature is less than five percent of the temperature differential applied across the substrate and the thermal reservoir. This small temperature increase is realized due to 1) the high thermal conductivity (~150 W/m·K) of silicon micro-cantilevers[65] as opposed to traditional silicon nitride micro-cantilevers that have very small thermal conductivity (~2 W/m·K)[92] and 2) the short length of the cantilever (~125 μm), which plays an important role in minimizing the heat flow from the substrate to the cantilever.

Appendix 2

Circuit for Voltage Amplifier

A schematic diagram of the voltage amplifier built to measure thermoelectric voltages of MMMJs is shown in Figure A2.1. It is based on a similar amplifier by Poler[72]. The gain of the amplifier is 250. Triaxial cables connect the AFM tip and the substrate to the amplifier box. The inner shield is driven at the same voltage as the core to reduce capacitive coupling with the environment. The operational amplifiers used were INA 116's, whose very high impedance limits the input bias currents to around 3 fA. The largest resistances encountered in the molecular junctions created for this work are 10 MΩ (for tetrabenzenethiol, S4). In this particular case, the offset voltage of the op amp would be 30 nV. This is orders of magnitude smaller than the thermoelectric voltages being read. The high input impedance allows for an accurate reading of these voltages.

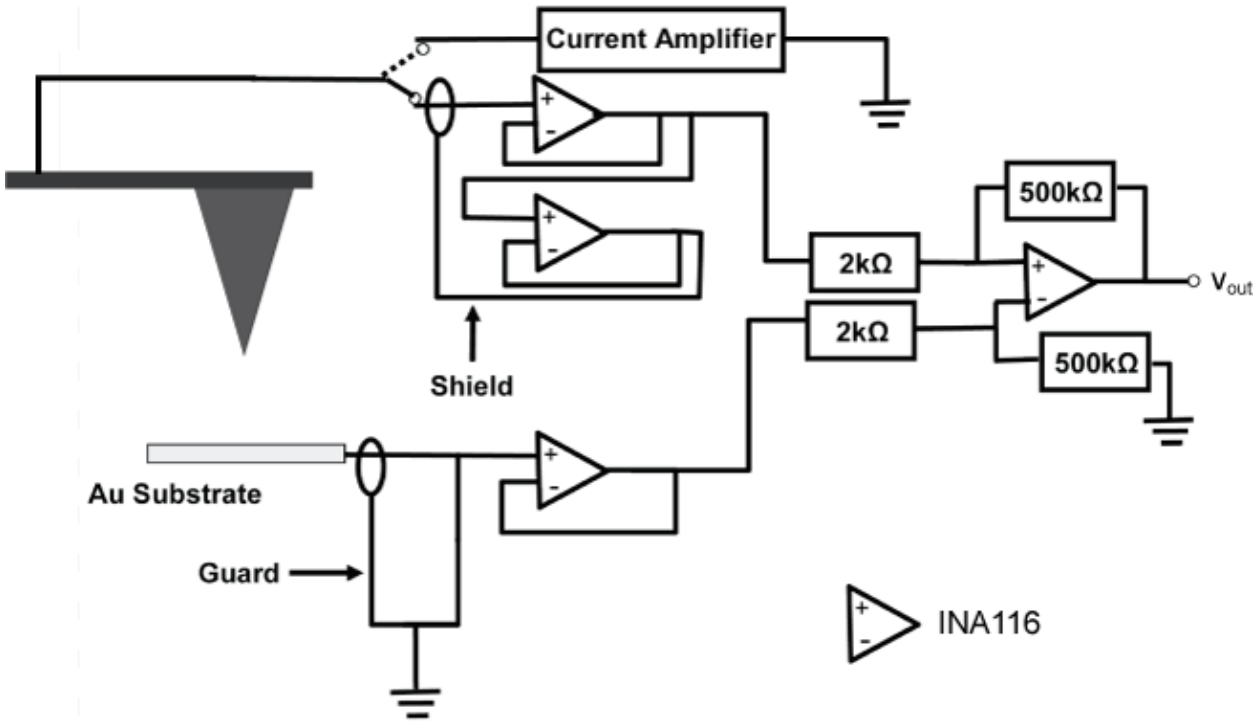

Figure A2.1 – Circuit diagram for the voltage amplifier used for reading thermoelectric voltages of molecular junctions.

Appendix 3

Sample Preparation

Gold Substrate Preparation

Gold substrates were prepared using a template stripping method[93,94]. Briefly, the process involved deposit 200 nm of gold onto a fresh Si wafer. Small drops of epoxy (Epo-Tek 377) are placed in a spaced configuration on top of the gold surface such that a 1 in^2 glass slide or silicon chip can be carefully placed on top of each epoxy drop. To obtain best results, the epoxy had to be stirred gently so that no air bubbles would form during the mixing of the two parts. The entire wafer (with epoxy and glass) is then placed into an oven and cured for 2 h at 150°C. Afterwards, a razor is used to dislodge a glass slide when a sample is needed. The gold remained adhered to the epoxy, and provides an ultra-flat substrate with a roughness of less than 1 nm over a 1 μm^2 area[83]. The cured template-stripped samples, if not exposed to the air, can be utilized even weeks after curing. If mixed gently, the cured epoxy can withstand immersion in weak solvents like ethanol for up to 48 hours without showing any signs of deformation or swelling.

AFM Tip Preparation

AFM tips were coated with alternating layers of chromium and gold (25 Å Cr, 50 Å Au, 25 Å Cr, 50 Å Au, 25 Å Cr, 100 Å Au, 25 Å Cr, 350 Å Au), following a recipe developed

by Morita and Lindsay[95]. This deposition method results in tips with a well defined radius (~75 nm) that allows for reliable and reproducible measurements.

FORMATION OF SELF-ASSEMBLED MONOLAYERS

All the molecules used in this study (Figure 2.8) were either purchased from Sigma Aldrich or synthesized by us. All thiol terminated molecules except tetrabenzenethiol were purchased from Sigma Aldrich. Tetrabenzenethiol was synthesized using a procedure given by Krapchetov[96], whereas terphenyl isocyanide was synthesized using a procedure developed by Henderson[70,97]. Monolayers were prepared by immersing Au substrates for ~24 hours in 1 mM solutions made in 200 proof ethanol (Decon Labs) or in toluene under an inert nitrogen environment.

MONOLAYER CHARACTERIZATION

Monolayers used in this work have all been previously verified and known to form well-ordered monolayers[68,69,98]. To ensure that this was the case for the samples used in our work, these samples were characterized by us using ellipsometry and X-ray photoelectron spectroscopy to determine thickness and chemical composition. A commercial ellipsometer (M-2000) by J. A. Woollam Co., Inc. was used to characterize the monolayers. Measurements were performed at three angles of incidence (55°, 65°, and 75°), over a wavelength range of 400 to 1600 nm. XPS experiments were performed with a Kratos Axis Ultra machine using a 8 mA and 14 kV monochromatic Al x-ray source. Thicknesses were calculated assuming an exponential attenuation of substrate photoelectrons due to the presence of the aromatic monolayer[64,74,93]. The attenuation length of Au photoelectrons were taken to be 42 Å, as reported by several groups for Au

$4f_{7/2}$ electrons passing through an organic film at ~1400 eV[99,100]. The two thickness measurement methods correlate well with each other (Table A3.1) and also correspond well with thicknesses reported in the published literature[35,74].

	S1	S2	S3	S4	NC3	SS1	SS2	SS3
Ellipsometry (nm)	0.40 (0.15)	1.40 (0.72)	1.60 (0.47)	1.88 (0.27)	1.70 (0.15)	0.75 (0.19)	1.34 (0.23)	1.61 (1.29)
XPS (nm)	0.51 (0.35)	1.01 (0.45)	1.27 (0.11)	1.46 (0.36)	1.67 (0.43)	1.10 (0.24)	1.50 (0.20)	1.72 (0.37)

Table A3.1 – Measured thickness of various self-assembled monolayers.

References

(1) Lane, P. *Organic Thin Films for Photonic Applications*; American Chemical Society, 2010; Vol. 1039.

(2) Burroughes, J. H.; Bradley, D. D. C.; Brown, A. R.; Marks, R. N.; Mackay, K.; Friend, R. H.; Burns, P. L.; Holmes, A. B. *Nature* **1990**, *347*, 539.

(3) Baldo, M. A.; O'Brien, D. F.; You, Y.; Shoustikov, A.; Sibley, S.; Thompson, M. E.; Forrest, S. R. *Nature* **1998**, *395*, 151.

(4) Tatsuo, H.; Jun, T. *Science and Technology of Advanced Materials* **2009**, *10*, 024314.

(5) Yoshiro, Y. *Science and Technology of Advanced Materials* **2009**, *10*, 024313.

(6) Liang, G. C.; Ghosh, A. W.; Paulsson, M.; Datta, S. *Physical Review B* **2004**, *69*, 115302.

(7) Günes, S.; Neugebauer, H.; Sariciftci, N. S. *Chemical Reviews* **2007**, *107*, 1324.

(8) Yu, G.; Gao, J.; Hummelen, J. C.; Wudl, F.; Heeger, A. J. *Science* **1995**, *270*, 1789.

(9) Aviram, A.; Ratner, M. A. *Chemical Physics Letters* **1974**, *29*, 277.

(10) Hush, N. S. *Annals of the New York Academy of Sciences* **2003**, *1006*, 1.

(11) Mulliken, R. S. *The Journal of Chemical Physics* **1939**, *7*, 14.

(12) Ferraris, J.; Walatka, V.; Perlstei.Jh; Cowan, D. O. *Journal of the American Chemical Society* **1973**, *95*, 948.

(13) Fischer, H.; Tom, G. M.; Taube, H. *Journal of the American Chemical Society* **1976**, *98*, 5512.

(14) Metzger, R. M.; Chen, B.; Höpfner, U.; Lakshmikantham, M. V.; Vuillaume, D.; Kawai, T.; Wu, X.; Tachibana, H.; Hughes, T. V.; Sakurai, H.; Baldwin, J. W.; Hosch, C.; Cava, M. P.; Brehmer, L.; Ashwell, G. J. *Journal of the American Chemical Society* **1997**, *119*, 10455.

(15) Salomon, A.; Cahen, D.; Lindsay, S.; Tomfohr, J.; Engelkes, V. B.; Frisbie, C. D. *Advanced Materials* **2003**, *15*, 1881.

(16) Wharam, D. A.; Thornton, T. J.; Newbury, R.; Pepper, M.; Ahmed, H.; Frost, J. E. F.; Hasko, D. G.; Peacock, D. C.; Ritchie, D. A.; Jones, G. A. C. *Journal of Physics C: Solid State Physics* **1988**, *21*, L209.

(17) van Wees, B. J.; van Houten, H.; Beenakker, C. W. J.; Williamson, J. G.; Kouwenhoven, L. P.; van der Marel, D.; Foxon, C. T. *Physical Review Letters* **1988**, *60*, 848.

(18) Imry, Y.; Landauer, R. *Reviews of Modern Physics* **1999**, *71*, S306.

(19) Landauer, R. *IBM J. Res. Dev.* **1957**, *1*, 223.

(20) Sherborne, B. S. *Journal of Physics: Condensed Matter* **1989**, *1*, 4825.

(21) Datta, S. *Quantum Transport: Atom to Transistor*; Cambridge University Press: New York, 2005.

(22) Quek, S. Y.; Venkataraman, L.; Choi, H. J.; Louie, S. G.; Hybertsen, M. S.; Neaton, J. B. *Nano Letters* **2007**, *7*, 3477.

(23) Markussen, T.; Chen, J.; Thygesen, K. S. *Physical Review B* **2011**, *83*, 155407.

(24) Paulsson, M.; Datta, S. *Physical Review B* **2003**, *67*, 241403.

(25) Wang, W.; Lee, T.; Reed, M. A. *Physical Review B* **2003**, *68*, 035416.

(26) Engelkes, V. B.; Beebe, J. M.; Frisbie, C. D. *Journal of the American Chemical Society* **2004**, *126*, 14287.

(27) Beebe, J. M.; Engelkes, V. B.; Miller, L. L.; Frisbie, C. D. *Journal of the American Chemical Society* **2002**, *124*, 11268.

(28) Wold, D. J.; Frisbie, C. D. *Journal of the American Chemical Society* **2000**, *122*, 2970.

(29) Wold, D. J.; Frisbie, C. D. *Journal of the American Chemical Society* **2001**, *123*, 5549.

(30) Wold, D. J.; Haag, R.; Rampi, M. A.; Frisbie, C. D. *The Journal of Physical Chemistry B* **2002**, *106*, 2813.

(31) Kasap, S. *Principles of Electronic Materials and Devices*; McGraw-Hill: New York, 2006.

(32) Kasap, S. *Thermoelectric effects in metals* **2001**, *kasap3.usask.ca/samples/Thermoelectric-Seebeck.pdf*.

(33) Butcher, P. N. *Journal of Physics: Condensed Matter* **1990**, *2*, 4869.

(34) Ashcroft, N. M., N. David *Solid State Physics*; Harcourt, Inc.: New York, 1976.

(35) Beebe, J. M.; Kim, B.; Gadzuk, J. W.; Daniel Frisbie, C.; Kushmerick, J. G. *Physical Review Letters* **2006**, *97*, 026801.

(36) Kim; Beebe, J. M.; Jun, Y.; Zhu, X. Y.; Frisbie, C. D. *Journal of the American Chemical Society* **2006**, *128*, 4970.

(37) Simmons, J. G. *Journal of Applied Physics* **1963**, *34*, 1793.

(38) Huisman, E. H.; Guédon, C. M.; van Wees, B. J.; van der Molen, S. J. *Nano Letters* **2009**, *9*, 3909.

(39) Chen, J.; Markussen, T.; Thygesen, K. S. *Physical Review B* **2010**, *82*, 121412.

(40) Nitzan, A.; Galperin, M.; Ingold, G.-L.; Grabert, H. *The Journal of Chemical Physics* **2002**, *117*, 10837.

(41) Mirjani, F.; Thijssen, J. M.; van der Molen, S. J. *Physical Review B* **2011**, *84*, 115402.

(42) Araidai, M.; Tsukada, M. *Physical Review B* **2010**, *81*, 235114.

(43) Xu, B.; Tao, N. J. *Science* **2003**, *301*, 1221.

(44) Venkataraman, L.; Klare, J. E.; Nuckolls, C.; Hybertsen, M. S.; Steigerwald, M. L. *Nature* **2006**, *442*, 904.

(45) Nitzan, A.; Ratner, M. A. *Science* **2003**, *300*, 1384.

(46) Chen, J.; Reed, M. A.; Rawlett, A. M.; Tour, J. M. *Science* **1999**, *286*, 1550.

(47) Song, H.; Kim, Y.; Jang, Y. H.; Jeong, H.; Reed, M. A.; Lee, T. *Nature* **2009**, *462*, 1039.

(48) Chabinyc, M. L.; Chen, X.; Holmlin, R. E.; Jacobs, H.; Skulason, H.; Frisbie, C. D.; Mujica, V.; Ratner, M. A.; Rampi, M. A.; Whitesides, G. M. *Journal of the American Chemical Society* **2002**, *124*, 11730.

(49) Lindsay, S. M.; Ratner, M. A. *Advanced Materials* **2007**, *19*, 23.

(50) Reed, M. A.; Zhou, C.; Muller, C. J.; Burgin, T. P.; Tour, J. M. *Science* **1997**, *278*, 252.

(51) Chen, J.; Calvet, L. C.; Reed, M. A.; Carr, D. W.; Grubisha, D. S.; Bennett, D. W. *Chemical Physics Letters* **1999**, *313*, 741.

(52) Zhou, C.; Deshpande, M. R.; Reed, M. A.; Jones Ii, L.; Tour, J. M. *Applied Physics Letters* **1997**, *71*, 611.

(53) Haag, R.; Rampi, M. A.; Holmlin, R. E.; Whitesides, G. M. *Journal of the American Chemical Society* **1999**, *121*, 7895.

(54) Holmlin, R. E.; Haag, R.; Chabinyc, M. L.; Ismagilov, R. F.; Cohen, A. E.; Terfort, A.; Rampi, M. A.; Whitesides, G. M. *Journal of the American Chemical Society* **2001**, *123*, 5075.

(55) Rampi, M. A.; Whitesides, G. M. *Chemical Physics* **2002**, *281*, 373.

(56) Park, J.; Pasupathy, A. N.; Goldsmith, J. I.; Chang, C.; Yaish, Y.; Petta, J. R.; Rinkoski, M.; Sethna, J. P.; Abruna, H. D.; McEuen, P. L.; Ralph, D. C. *Nature* **2002**, *417*, 722.

(57) Kushmerick, J. G.; Holt, D. B.; Pollack, S. K.; Ratner, M. A.; Yang, J. C.; Schull, T. L.; Naciri, J.; Moore, M. H.; Shashidhar, R. *Journal of the American Chemical Society* **2002**, *124*, 10654.

(58) Kushmerick, J. G.; Holt, D. B.; Yang, J. C.; Naciri, J.; Moore, M. H.; Shashidhar, R. *Physical Review Letters* **2002**, *89*, 086802.

(59) Beebe, J. M.; Kim, B.; Frisbie, C. D.; Kushmerick, J. G. *ACS Nano* **2008**, *2*, 827.

(60) Binnig, G.; Rohrer, H.; Gerber, C.; Weibel, E. *Physical Review Letters* **1982**, *49*, 57.

(61) Binnig, G.; Quate, C. F.; Gerber, C. *Physical Review Letters* **1986**, *56*, 930.

(62) Bumm, L. A.; Arnold, J. J.; Cygan, M. T.; Dunbar, T. D.; Burgin, T. P.; Ii, L. J.; Allara, D. L.; Tour, J. M.; Weiss, P. S. *Science* **1996**, *271*, 1705.

(63) Lee, W.; Reddy, P. *Nanotechnology* **2011**, *22*, 485703.

(64) Tan, A.; Sadat, S.; Reddy, P. *Applied Physics Letters* **2010**, *96*, 013110.

(65) Incropera, F. P. *Fundamentals of Heat and Mass Transfer*; 6 ed.; John Wiley, 2007.

(66) Shi, L.; Majumdar, A. *Journal of Heat Transfer* **2002**, *124*, 329.

(67) Johnson, K. L. *Contact Mechanics*; Cambridge University Press, 1985.

(68) Dubois, L. H.; Nuzzo, R. G. *Annual Review of Physical Chemistry* **1992**, *43*, 437.

(69) Love, J. C.; Estroff, L. A.; Kriebel, J. K.; Nuzzo, R. G.; Whitesides, G. M. *Chemical Reviews* **2005**, *105*, 1103.

(70) Hong, S.; Reifenberger, R.; Tian, W.; Datta, S.; Henderson, J. I.; Kubiak, C. P. *Superlattices and Microstructures* **2000**, *28*, 289.

(71) Choi, S. H.; Risko, C.; Delgado, M. C. R.; Kim, B.; Brédas, J.-L.; Frisbie, C. D. *Journal of the American Chemical Society* **2010**, *132*, 4358.

(72) Poler, J. C.; Zimmermann, R. M.; Cox, E. C. *Langmuir* **1995**, *11*, 2689.

(73) Weber, L.; Lehr, M.; Gmelin, E. *Physica B: Condensed Matter* **1996**, *217*, 181.

(74) Reddy, P.; Jang, S.-Y.; Segalman, R. A.; Majumdar, A. *Science* **2007**, *315*, 1568.

(75) Ke, S.-H.; Baranger, H. U.; Yang, W. *Journal of the American Chemical Society* **2004**, *126*, 15897.

(76) Mishchenko, A.; Zotti, L. A.; Vonlanthen, D.; Bürkle, M.; Pauly, F.; Cuevas, J. C.; Mayor, M.; Wandlowski, T. *Journal of the American Chemical Society* **2010**, *133*, 184.

(77) Xue, Y.; Datta, S.; Ratner, M. A. *Chemical Physics* **2002**, *281*, 151.

(78) Xue, Y.; Ratner, M. A. *Physical Review B* **2004**, *69*, 085403.

(79) Zotti, L. A.; Kirchner, T.; Cuevas, J.-C.; Pauly, F.; Huhn, T.; Scheer, E.; Erbe, A. *Small* **2010**, *6*, 1529.

(80) Baheti, K.; Malen, J. A.; Doak, P.; Reddy, P.; Jang, S.-Y.; Tilley, T. D.; Majumdar, A.; Segalman, R. A. *Nano Letters* **2008**, *8*, 715.

(81) Malen, J. A.; Doak, P.; Baheti, K.; Tilley, T. D.; Majumdar, A.; Segalman, R. A. *Nano Letters* **2009**, *9*, 3406.

(82) Malen, J. A.; Doak, P.; Baheti, K.; Tilley, T. D.; Segalman, R. A.; Majumdar, A. *Nano Letters* **2009**, *9*, 1164.

(83) Engelkes, V. B.; Beebe, J. M.; Frisbie, C. D. *The Journal of Physical Chemistry B* **2005**, *109*, 16801.

(84) King, G. M.; Carter, A. R.; Churnside, A. B.; Eberle, L. S.; Perkins, T. T. *Nano Letters* **2009**, *9*, 1451.

(85) RHK *http://www.rhk-tech.com/downloads_files_V2.php#product*.

(86) Finch, C. M.; García-Suárez, V. M.; Lambert, C. J. *Physical Review B* **2009**, *79*, 033405.

(87) Aleksei, V. D.; Igor, P. Z. *Physics-Uspekhi* **2010**, *53*, 789.

(88) Harman, T.; Walsh, M.; laforge, B.; Turner, G. *Journal of Electronic Materials* **2005**, *34*, L19.

(89) Ge, Z.; Cahill, D. G.; Braun, P. V. *Physical Review Letters* **2006**, *96*, 186101.

(90) Wang, R. Y.; Segalman, R. A.; Majumdar, A. *Applied Physics Letters* **2006**, *89*, 173113.

(91) Rohsenow, W. C., H. *Heat, Mass, and Momentum Transfer*; Prentice-Hall: Englewood Cliffs, NJ, 1961.

(92) von Arx, M.; Paul, O.; Baltes, H. *Microelectromechanical Systems, Journal of* **2000**, *9*, 136.

(93) Blackstock, J. J.; Li, Z.; Freeman, M. R.; Stewart, D. R. *Surface Science* **2003**, *546*, 87.

(94) Wagner, P.; Hegner, M.; Guentherodt, H.-J.; Semenza, G. *Langmuir* **1995**, *11*, 3867.

(95) Morita, T.; Lindsay, S. *Journal of the American Chemical Society* **2007**, *129*, 7262.

(96) Krapchetov, D. A.; Ma, H.; Jen, A. K. Y.; Fischer, D. A.; Loo, Y.-L. *Langmuir* **2005**, *21*, 5887.

(97) Henderson, J. I.; Feng, S.; Bein, T.; Kubiak, C. P. *Langmuir* **2000**, *16*, 6183.

(98) Tour, J. M.; Jones, L.; Pearson, D. L.; Lamba, J. J. S.; Burgin, T. P.; Whitesides, G. M.; Allara, D. L.; Parikh, A. N.; Atre, S. *Journal of the American Chemical Society* **1995**, *117*, 9529.

(99) Bain, C. D.; Whitesides, G. M. *The Journal of Physical Chemistry* **1989**, *93*, 1670.

(100) Lu, Q.; Liu, K.; Zhang, H.; Du, Z.; Wang, X.; Wang, F. *ACS Nano* **2009**, *3*, 3861.